

Coupled Phenomena (3rd year, LEAer)
Academic Year 21/22

Multipole Series of Gravity and Other Fields

Group #4
Alano Silva, nº 83659
Diogo Faustino, nº 95782
Henry Machado, nº 95795
João Soeiro, nº 95803
José Bento, nº 95815
Rúben Novais, nº 95843
Tomás Nunes, nº 95855
Rodrigo Sequeira, nº 96480

Abstract

Gravity field expressions that can take into account the true shape of the celestial body are derived from Laplace's equation, the result being the spherical harmonic gravity field. Each term of the spherical harmonic expansion has a physical meaning that can be traced back to the shape of the body. This gravity field is said to be the exterior spherical harmonic gravity field, as its convergence region is outside the Brillouin sphere of the body. The exterior spherical harmonic gravity field cannot model the gravitation within the exterior Brillouin sphere except in some special cases. So, in this report, we will also discuss different models for the interior gravity field expressions. We apply the theory to the development of a Python program that simulates the geopotential, approximates a bodies' surface with the multipole expansion and also represents the different spherical harmonics. We were also able to build a model of the surface of the earth from available coefficients. A comparison is made with existing models, as we analyse some popular approximations for the surface of the Earth and the meaning of the GOCE space probe in the context of our work.

Keywords: multipole series expansion, spherical harmonics, geopotential, geodesy, gravitational field

Acknowledgements

We sincerely thank our Course Instructor, Paulo J. S. Gil, for the much needed guidance both during the development of this project report and in the preparation for the lecture given.

Contents

1	Introduction	4
2	Poisson and Laplace's equation	5
2.1	Solution of Poisson's equation in integral form	5
3	Solution of Laplace's equation	7
3.1	Legendre Polynomials	9
3.2	Spherical Harmonics	11
4	The Addition Theorem for Spherical Harmonics	14
4.1	Proof of the Addition Theorem	15
5	Geopotential Expansion	16
5.1	The Normalized Geopotential Coefficients	17
6	Physical interpretation of spherical harmonics	17
6.1	Zonal, Sectorial and Tesselal terms	17
6.2	Spherical Harmonics' Completeness	20
6.3	Spherical Harmonics in Quantum Physics	21
7	Shell theorem	22
7.1	Proof of Newton's Shell Theorem	22
8	Gauss's Law	24
8.1	Gauss's Law derivation	25
8.2	Gravitational field inside the Earth for different density models	26
8.3	Comparison with more realistic model	27
9	Journey to the center of the Earth	28
9.1	Simple harmonic motion	28
10	Geodesy	29
10.1	Earth seen as an ellipsoid of revolution	30
10.2	The reference ellipsoid	30
10.3	The geoid	31
10.4	Undulation	32
11	Method of Least Squares	33
12	Program	34
12.1	Representing a body's surface using spherical harmonics	35
12.2	Calculating Gravitational Potential and some characteristics of the Earth's geoid	38

13 Earth's geoid analysis with computational program	39
13.1 Representing the geoid from known spherical harmonics coefficients	40
13.2 Individual contribution of spherical harmonics terms	41
13.3 Analysis of higher order terms	42
14 Analysis of the Earth's gravitational potential field with computational program	44
14.1 Potential in a surface of constant radius outside the planet	44
14.2 Potential in a plane that passes through the center of the Earth	46
15 GOCE space probe	47
15.1 The mission	48
15.2 SST-hl technique	49
15.3 Instrumentation	50
15.4 Data Processing	51
15.5 Least-squares adjustment	52
15.6 Model Recovery	54
16 Conclusion	57
<i>References</i>	58
Appendix A Expansion in spherical harmonics and their completeness	60
Appendix B Program Guide	62
Appendix B.1 Installation instructions	62
Appendix B.2 Features	63
Appendix C Group qualitative assessment	71

1. Introduction

Newton's law of universal gravitation is sufficiently accurate for many practical purposes and is therefore widely used. If we construct the gravity field by approximating the Earth to a sphere with homogeneous mass distribution that is equivalent to a point mass, we miss out on the true richness of the Earth's gravitational potential. That is the main goal of our work, to construct a more realistic gravitational potential for an arbitrarily shaped body by approaching it as a multipole instead of the usual monopole approximation. The multipole series expansion allows us to take into account the true shape of the Earth as well as the changes in density in the Earth's interior.

A multipole expansion is a mathematical series representing a function that depends on angles: usually the two angles used in the spherical coordinate system (the polar and azimuthal angles). Similarly to a Taylor series, multipole expansions are useful because oftentimes only the first few terms are needed to provide a good approximation of the original function. For this reason, they are used frequently in the study of electromagnetic and gravitational fields. The multipole expansion with angles is often combined with an expansion in radius. Such a combination gives an expansion describing a function throughout three-dimensional space.

Our goal for this work is precisely that, to construct and explore the characteristics of the gravitational field around an arbitrary body. We will present particular solutions of notable cases, explore the region of validity for the model presented (outside of a circumscribing sphere), find alternative ways to determine gravitational fields on the interior of said sphere and show some computational simulations of the surfaces of real celestial bodies, whose information was taken from the NASA website. This is done because in order to use spherical harmonics to describe the gravitational field around a celestial body we must have accurate information of both its surface and its density distribution to compute the expansion coefficients. If we assume homogeneity, the mass distribution is much easier to evaluate and so we can create a gravity model. To conclude, we analyse some popular approximations for the surface of the Earth, such as the reference ellipsoid and the geoid, and explore the importance of the GOCE space probe in the discovery of the Earth's gravity coefficients.

2. Poisson and Laplace's equation

The behavior of the gravity field \mathbf{g} can be described by the two differential equations:

$$\nabla \cdot \mathbf{g} = 4\pi G\rho \quad (1)$$

$$\nabla \times \mathbf{g} = 0 \quad (2)$$

The expression 2 is equivalent to the statement that \mathbf{g} is the gradient of a scalar function. The scalar potential φ satisfies:

$$\mathbf{g} = -\nabla\varphi \quad (3)$$

We can, therefore, write the gravity field as being equal to the Laplacian ∇^2 of the scalar potential, as follows:

$$\nabla \cdot \mathbf{g} = \nabla \cdot (-\nabla\varphi) = -\nabla^2\varphi \quad (4)$$

$$\nabla^2\varphi = -\nabla \cdot \mathbf{g} \quad (5)$$

Rearranging the terms on the equations, we get:

$$\nabla^2\varphi = -4\pi G\rho \quad (6)$$

where G is the universal gravity constant. This formula is known as the **Poisson equation** for gravity fields. In regions of space where there is no mass density ρ , the scalar potential satisfies the **Laplace equation**:

$$\nabla^2\varphi = 0 \quad (7)$$

2.1. Solution of Poisson's equation in integral form

Our goal is to accurately study the Earth's gravitational potential, a potential that obviously fulfills the Poisson equation. So how can we determine and express such potential? To simplify our calculations, we normally assume that the total mass of the Earth is concentrated in the center of the coordinate system, and the gravitational law

$$\ddot{\mathbf{r}} = -\frac{GM_{\oplus}}{r^3}\mathbf{r} \quad (8)$$

can be used to calculate the acceleration of a body at distance \mathbf{r} . For the following discussion of a more realistic model, we shall use a representation involving the gradient of the corresponding gravity potential U , as follows:

$$\ddot{\mathbf{r}} = -\nabla U \quad (9)$$

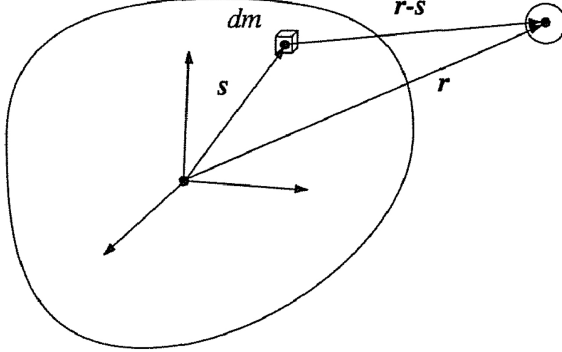


Figure 1: The contribution of a small mass element to the potential [1].

with

$$U = GM_{\oplus} \frac{1}{r}. \quad (10)$$

This expression for the potential may easily be generalized to an arbitrary mass distribution by summing up the contributions created by individual mass elements $dm = \rho(s)d^3s$ according to [1]:

$$U = G \int \frac{\rho(\vec{s})d^3s}{|\vec{r} - \vec{s}|}. \quad (11)$$

Here, $\rho(s)$ means the density at some point s inside the Earth, and $|\vec{r} - \vec{s}|$ is the distance between the test point (the point at which we are calculating the potential) and said point s , as shown in figure 1.

We will now briefly prove the integral in equation 11 does indeed fulfill the Poisson equation. We do this by applying the Laplacian to both sides of equation 11, and we get this simplified new equation:

$$\nabla^2 \Phi = G \int \rho(\vec{s}) \nabla^2 \left(\frac{1}{|\vec{r} - \vec{s}|} \right) d^3s. \quad (12)$$

It is known that the Laplacian term present in the integral of equation 12 is equal to the following product, $-4\pi\delta(\vec{r} - \vec{s})$, where δ is the Dirac delta function [2]. There is no need to study in depth all the concepts and properties of this function, as it would most likely lead to a long and extensive essay that far outreaches the goals we have proposed for ourselves. That being said, just to give some context about the Dirac delta function, over the reals, this function is null for every point except the origin ($x=0$) and the integral of this function over the entire real line is equal to 1 (this function represents an "impulse") [3].

Continuing our proof, let's now incorporate the Dirac function in equation 12:

$$\nabla^2 \Phi = -4\pi G \int \rho(\vec{s}) \delta(\vec{r} - \vec{s}) d^3s. \quad (13)$$

We still need to dismantle that Laplacian term. The Dirac delta function has a "sifting" property that goes like this [3],

$$\int \rho(\vec{s})\delta(\vec{r} - \vec{s})d^3s = \rho(\vec{r}), \quad (14)$$

showing that the entire integral term of equation 13 is no more than the mass density, now dependent on the radius, \vec{r} . Substituting then the integral term of equation 13 by the result of equation 14, we get Poisson's equation (equation 6), completing our proof. We want to develop and simplify the expression for the gravitational potential, which is for now in integral form (equation 11). In order to do this, we need to learn and consolidate some concepts first. We will start by solving the simplified case of the Laplace equation.

3. Solution of Laplace's equation

We'll be solving Laplace's equation in spherical coordinates. We will mostly follow the derivation presented in the book "Classical Electrodynamics", from the authorship of J.D. Jackson (starting from page 84 until page 87, then from pages 98 to 100, [2]). We're interested in finding a solution to a gravitational potential, and, using Earth as an example, the approximate form we use is dependant on a distance, r , between a test object (a satellite, for example) and Earth's center of mass - the coordinates system that best suits these conditions is the spherical one. We now present Laplace's equation in spherical coordinates,

$$\frac{1}{r} \frac{\partial^2}{\partial r^2}(r\Phi) + \frac{1}{r^2 \sin \theta} \frac{\partial}{\partial \theta}(\sin \theta \frac{\partial \Phi}{\partial \theta}) + \frac{1}{r^2 \sin^2 \theta} \frac{\partial^2 \Phi}{\partial \phi^2} = 0, \quad (15)$$

where r is the radius, θ is the polar angle measured from the z-axis and ϕ is the azimuthal angle, varying from 0 to 2π .

We'll use a variable separation method, where we assume our potential, Φ , to be the product of three separate potentials, each one dependent on each one of the spherical coordinate variables:

$$\Phi = \frac{U(r)}{r} P(\theta) Q(\phi). \quad (16)$$

The potential part dependent on the radius, r , isn't solely U because that would complicate our math going forward. This product solution of the potential is now input on equation 15 and we get a new, more simplified version of the same equation:

$$r^2 \sin^2 \theta \frac{1}{U} \frac{d^2 U}{dr^2} + \sin \theta \frac{1}{P} \frac{d}{d\theta}(\sin \theta \frac{dP}{d\theta}) + \frac{1}{Q} \frac{d^2 Q}{d\phi^2} = 0. \quad (17)$$

It is noticeable that in comparison to equation 15, which is full of partial derivatives, equation 17 no longer has partial derivatives, only total derivatives, which will allow us to solve the linear differential equations for each potential with more ease.

Analyzing equation 17, we are presented with a sum of three terms: the first two terms have dependence on r and θ , while the third term has dependence on ϕ . Therefore, through

the perspective of the potential Q , the sum of the two first terms is a constant, and since the global sum is zero, the third term is also a constant. This constant will be called $-m^2$ (it will be quite intuitive why that is). This translates into a second-order liner differential equation,

$$\frac{1}{Q} \frac{d^2Q}{d\phi^2} = -m^2, \quad (18)$$

which is fairly simple to solve, yielding the following solution:

$$Q = e^{\pm im\phi}. \quad (19)$$

Important to note that since the azimuthal angle, ϕ , is a periodic variable, the potential Q must then be a periodical function. This condition can be translated to the following equation,

$$Q(\phi) = Q(\phi + 2\pi) \Leftrightarrow e^{\pm im\phi} = e^{\pm im\phi} \cdot e^{\pm i2\phi m}, \quad (20)$$

which tells us that the condition is fulfilled if m is an integer.

With the potential Q discovered, we can go back to equation 17 and rearrange it, in order to isolate all radius dependent terms on one side, in order to find the expression for the radius potential U :

$$\frac{r^2}{U} \frac{d^2U}{dr^2} = \frac{m^2}{\sin^2 \theta} - \frac{1}{P \sin \theta} \frac{d}{d\theta} (\sin \theta \frac{dP}{d\theta}). \quad (21)$$

Once again, if the left term is only dependent on the radius, r , and the right term is not dependent on it, then this right term must be a constant. This constant will be called $l(l+1)$ (once again it will become intuitive to why this is), giving us another second-order linear differential equation,

$$\frac{d^2U}{dr^2} = -\frac{l(l+1)}{r^2} U. \quad (22)$$

This equation though is different from 18, since it obeys to the following canonical form, where the coefficients are no longer constants (as it is the case in equation 18) but actually simple polynomials:

$$ax^2y''(x) + bxy'(x) + cy(x) = 0. \quad (23)$$

This is called an Euler equation and its solution is a power function, cx^s , so the exponent s is the parameter to be determined (and there can be more than one solution to it) [4]. We just need to input this solution type into equation 22 and solve it for s . The output is that the exponent s can either take the value of l or $l + 1$, meaning the solution to the radius dependent potential U is the following power series,

$$U = Ar^{l+1} + Br^{-l}. \quad (24)$$

Since the solution is a power series, the exponents must be integers, meaning that the constant l must be an integer (just like m).

3.1. Legendre Polynomials

We now have only one potential expression left to find, the P potential one. Returning to equation 21, we can eliminate dependence on the radius, r , since the left term is now equal to $l(l + 1)$, culminating in a solely dependent on the polar angle θ equation:

$$\frac{1}{\sin \theta} \frac{d}{d\theta} (\sin \theta \frac{dP}{d\theta}) - [\frac{m^2}{\sin^2 \theta} - l(l + 1)]P. \quad (25)$$

This equation though is normally expressed for the cosine of the polar angle, θ ($x = \cos \theta$), and is named the Legendre equation:

$$\frac{d}{dx} [(1 - x^2) \frac{dP}{dx}] + [l(l + 1) - \frac{m^2}{1 - x^2}]P = 0. \quad (26)$$

The solutions for this equation are the Legendre polynomials, which are dependent on l , which we will call the degree, and m , which will be the order.

We'll start by studying the zero order Legendre polynomials. It is very important to note that we need the solution to the Legendre equation to be single-valued, finite and continuous on its interval ($[-1 ; 1]$) in order to proper represent a physical potential. In order for this to happen it can be proven that the degree, l , needs to be non-negative (this is proven (dare I say alluded) very loosely in page 86 of "Classical Electrodynamics" [2]). Moving forward, we now hereby present the first (low degree) zero order Legendre polynomials, which are also graphically represented in figure 2:

$$\begin{aligned} P_0(x) &= 1; \\ P_1(x) &= x; \\ P_2(x) &= \frac{1}{2}(3x^2 - 1); \\ P_3(x) &= \frac{1}{2}(5x^3 - 3x); \\ P_4(x) &= \frac{1}{8}(35x^4 - 30x^2 + 3). \end{aligned} \quad (27)$$

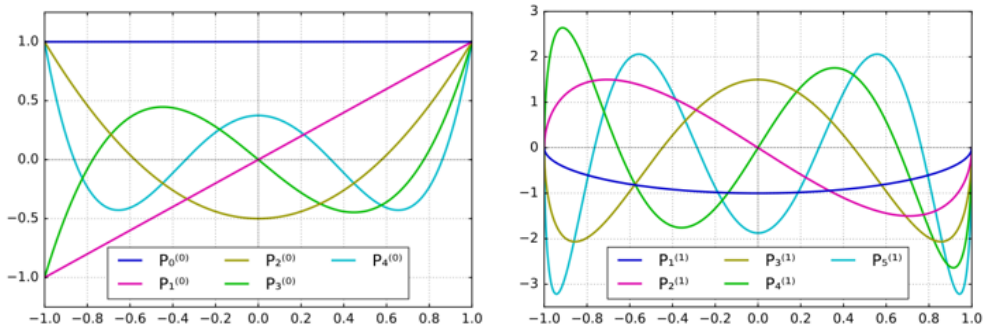


Figure 2: Low degree Legendre polynomials of order 0 (left) and 1 (right) [5].

Since x is the cosine of the angle θ , the domain of these polynomials ranges from -1 to 1. Plus, by convention, these polynomials are normalized to have the unity value at $x=1$, as it is noticeable at the left of figure 2. It also becomes very clear by analysing that same graph that the polynomials with an even degree (0,2,4,...) are even functions and polynomials with an odd degree (1,3,...) are odd functions. A formula can be obtained to calculate these functions, the Rodrigues formula:

$$P_l(x) = \frac{1}{2^l l!} \frac{d^l}{dx^l} (x^2 - 1)^l. \quad (28)$$

For values of m different than zero, the solutions to the Legendre equation are the Associate Legendre functions. Once again, in order for these solutions to be finite, single-valued and continuous on their domain, not only does the degree, l , must be superior to zero, but the order, m , needs to belong to the following range, $\{-l; -(l-1); \dots; 0; \dots; l-1; l\}$. This can be proved in similar fashion to the proof in appendix). The Legendre functions for positive order can be calculated through

$$P_l^m(x) = (-1)^m (1-x^2)^{\frac{m}{2}} \frac{d^m}{dx^m} P_l(x), \quad (29)$$

and we can use a modified equation 29 to determine the functions of negative order -

$$P_l^{-m}(x) = (-1)^m \frac{(l-m)!}{(l+m)!} P_l^m(x), \quad (30)$$

for $m > 0$.

Going back to figure 2, in the graph to the right we have presented the low degree first order Legendre polynomials. These polynomials no longer tend to 1 at $x = 1$. Instead, they tend to zero (have a node) in each of the domain boundaries (-1 and 1). It is noticeable in this graph that the criteria for parity of these functions is different - polynomials with an odd degree are even functions while the ones with an even degree are odd functions. The parity of the Legendre polynomials is then dependent on both the degree, l , and the order, m :

$$P_l^m(-x) = (-1)^{l+m} P_l^m(x). \quad (31)$$

This way, if the sum $l+m$ is odd, the Legendre function is odd, if it is even, the function is even [5].

These Legendre functions carry a very important property - orthogonality. For a fixed m , the Legendre polynomials form a complete set of orthogonal functions, meaning that any well-behaved function can be expanded in terms of these functions, on the $[-1;1]$ domain (in simpler terms, the Legendre functions form an infinite orthogonal base):

$$f(x) = \sum_{l=0}^{\infty} A_l P_l(x). \quad (32)$$

The orthogonal relation is given by

$$\int_{-1}^1 P_{l'}^m(x) P_l^m(x) dx = \frac{2}{2l+1} \frac{(l+m)!}{(l-m)!} \delta_{l'l}, \quad (33)$$

confirming that any two different Legendre functions (of same order) are orthogonal (the numerical value of the previous integral is zero). The fact that the numerical value of the same integral is capable of being different than 1 for Legendre functions of the same degree means that this base is not orthonormal.

Now that we have studied the Legendre polynomials, which are the solutions to the polar angle, θ , dependent potential, P , we have figured out all three potentials (U , P and Q). Therefore, we could right away introduce the final solution to the Laplace equation, but it is of our interest to first introduce a new concept.

3.2. Spherical Harmonics

It is a good practice to combine the "angular" potentials. We have approached the orthogonality of the Legendre functions. The solutions to the Q potential, given by equation 19, form a complete set of orthogonal functions in the index m on their domain (the azimuthal angle ϕ varies from 0 to 2π). This means the product of the two potentials, PQ , will form a complete set of orthogonal functions on the surface of a sphere. These functions are called spherical harmonics, are denoted by the letter Y , and can be calculated for each degree, l , and order, m , by the following expression:

$$Y_{lm}(\theta, \phi) = \sqrt{\frac{2l+1}{4\pi} \frac{(l-m)!}{(l+m)!}} P_l^m(\cos \theta) e^{im\phi}. \quad (34)$$

The square root term is a normalization factor, in this case it does indeed normalize the set of orthogonal functions that constitutes the spherical harmonics, meaning we now get a complete set of orthonormal functions over the unit sphere, which can be beneficial for some applications (acoustics, for example). In figure 3, we have presented the algebraic expressions for the first spherical harmonics (with orthonormal normalization):

Spherical harmonics $\mathbf{Y}_{lm}(\theta, \phi)$

$$\begin{aligned}
l=0 \quad & Y_{00} = \frac{1}{\sqrt{4\pi}} \\
l=1 \quad & \left\{ \begin{array}{l} Y_{11} = -\sqrt{\frac{3}{8\pi}} \sin \theta e^{i\phi} \\ Y_{10} = \sqrt{\frac{3}{4\pi}} \cos \theta \end{array} \right. \\
& Y_{22} = \frac{1}{4} \sqrt{\frac{15}{2\pi}} \sin^2 \theta e^{2i\phi} \\
l=2 \quad & Y_{21} = -\sqrt{\frac{15}{8\pi}} \sin \theta \cos \theta e^{i\phi} \\
& Y_{20} = \sqrt{\frac{5}{4\pi}} (\frac{3}{2} \cos^2 \theta - \frac{1}{2}) \\
l=3 \quad & \left\{ \begin{array}{l} Y_{33} = -\frac{1}{4} \sqrt{\frac{35}{4\pi}} \sin^3 \theta e^{3i\phi} \\ Y_{32} = \frac{1}{4} \sqrt{\frac{105}{2\pi}} \sin^2 \theta \cos \theta e^{2i\phi} \\ Y_{31} = -\frac{1}{4} \sqrt{\frac{21}{4\pi}} \sin \theta (5 \cos^2 \theta - 1) e^{i\phi} \\ Y_{30} = \sqrt{\frac{7}{4\pi}} (\frac{5}{2} \cos^3 \theta - \frac{3}{2} \cos \theta) \end{array} \right.
\end{aligned}$$

Figure 3: Low degree spherical harmonics (orthonormal normalization) [2].

In order to calculate the spherical harmonics' functions of negative order, m , we make use of the conjugate spherical harmonics, Y_{lm}^* :

$$Y_{l,-m}(\theta, \phi) = (-1)^m Y_{lm}^*(\theta, \phi). \quad (35)$$

Just as it was the case with the Legendre polynomials, we can judge the parity of the spherical harmonics' functions. These functions are defined based on spherical coordinates, so first we need to address the parity transformation of such coordinates. This transformation is fundamentally the same as the cartesian coordinates' transformation. In cartesian coordinates we compare the function value between a generic point, (x, y, z) and its symmetric in relation to the origin, $(-x, -y, -z)$. The principle is the same for spherical coordinates, it is just a case of defining the symmetrical point in spherical coordinates, which is quite intuitive to do just by visualizing the unit sphere. The parity transformation for this coordinates set is then given by:

$$(r, \theta, \phi) \longrightarrow (r, \pi - \theta, \pi + \phi). \quad (36)$$

The spherical harmonics' functions are only dependent on the angular coordinates, and so the parity of such functions is expressed by the following relation:

$$Y_{l,m}(\pi - \theta, \pi + \phi) = (-1)^l Y_{lm}(\theta, \phi). \quad (37)$$

The parity of these functions is thus only dependent on their degree, l . Spherical harmonics' functions of an odd degree are odd and those with an even degree are even [6]. This property

is more important and greater explored in the realm of quantum mechanics (which we are not interested in exploring on this essay), so we won't go deeper on this specific subject.

Finally, but not least, the spherical harmonics form not only an orthogonal set of functions, but a complete set of orthogonal functions, as we have slightly touched upon. This means that, if you think of the set of spherical harmonic functions as a base, all these functions are linearly independent, which translates to there being no function (not belonging to the set) that is orthogonal to all the spherical harmonic functions belonging to the set [7]. Despite being counter-intuitive, we can define linear independence of an infinite set of vectors (or functions): if every nonempty finite subset of said set is linearly independent, the infinite vector set is linearly independent. For example, the infinite set of functions $\{1, x, x^2, x^3, \dots\}$ is linearly independent and forms a base on the vector space of all polynomials. Since the spherical harmonics' functions form a complete set of orthogonal functions, we can expand any well behaved function of the polar angle, θ , and the azimuth angle, ϕ in a spherical harmonics' series

$$g(\theta, \phi) = \sum_{l=0}^{\infty} \sum_{m=-l}^l A_{lm} Y_{lm}(\theta, \phi), \quad (38)$$

and the coefficients A_{lm} can be determined with the following integral,

$$A_{lm} = \int d\Omega Y_{lm}^*(\theta, \phi) g(\theta, \phi), \quad (39)$$

where $d\Omega$ is the differential solid angle. In appendix Appendix A we approach the meaning of well behaved function in context of the spherical harmonics and we proof the completeness of their set.

Now that we have studied spherical harmonics and their properties, we can finally present the solution to Laplace's equation, using spherical harmonics:

$$\Phi(r, \theta, \phi) = \sum_{l=0}^{\infty} \sum_{m=-l}^l [A_{lm} r^l + B_{lm} r^{-(l+1)}] Y_{lm}(\theta, \phi). \quad (40)$$

The coefficients A_{lm} and B_{lm} can be determined through boundary conditions on a spherical surface. Considering the example of a gravitational potential, we know this potential tends to zero for infinite distances from the center of mass that generates the potential. If we analyse equation 40, we noticed that as we tend for terms of infinite degree, l , the two components of the radial potential show different behaviours: the one preceded by the coefficient A tends to infinity for great values of r and the one preceded by the coefficient B tends to zero for great values of r . Given what we have stated before about the potential for infinite values of radius, r , it is quite intuitive and easy to predict that the coefficient(s) A_{lm} will be null, in order to eradicate that first component of the radial potential which doesn't mathematically mirror the physics of reality. Before we can expand the Earth's gravitational potential in a spherical harmonics' series, there is still a very useful property of this set of functions left to study and master.

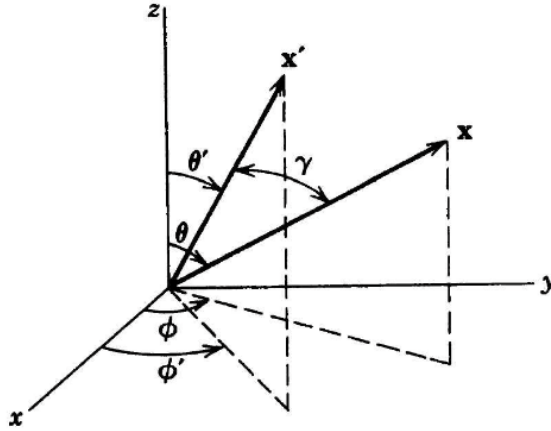


Figure 4: The two vectors \vec{r} and \vec{s} are denoted in this figure by x and x' , respectively. The angle between the two vectors is denoted by γ

4. The Addition Theorem for Spherical Harmonics

A mathematical result of considerable interest and use is called the addition theorem for spherical harmonics. Two coordinate vectors \mathbf{r} and \mathbf{s} , with spherical coordinates (r, θ, φ) and (r', θ', φ') , respectively, have an angle γ between them, as shown in the figure 4.

The angle γ between the two vectors is easily computed. Noting that the unit vector \hat{r} is given by:

$$\hat{r} = \frac{\vec{r}}{r} = \hat{\mathbf{i}} \sin \theta \cos \phi + \hat{\mathbf{j}} \sin \theta \sin \phi + \hat{\mathbf{k}} \cos \theta \quad (41)$$

and similarly, for \hat{s} , it follows that:

$$\cos \gamma = \hat{r} \cdot \hat{s} = \cos \theta \cos \theta' + \sin \theta \sin \theta' \cos (\varphi - \varphi') \quad (42)$$

The addition theorem expresses a Legendre polynomial of order l in the angle γ in terms of products of the spherical harmonics of the angles θ, φ and θ', φ' :

$$P_l(\cos \gamma) = \frac{4\pi}{2l+1} \sum_{m=-l}^l Y_{lm}^*(\theta', \varphi') Y_{lm}(\theta, \varphi) \quad (43)$$

where $\cos \gamma$ is given by (42). We are also going to consider another form of this theorem, given by the following expression:

$$P_n(\cos \gamma) = \sum_{m=0}^n (2 - \delta_{0m}) \frac{(n-m)!}{(n+m)!} P_{nm}(\sin \varphi) P_{nm} \sin \varphi' \cos(m(\theta - \theta')) \quad (44)$$

Here, P_{nm} are the associated Legendre polynomial of degree n and order m , and the angles θ and ϕ are the spherical angles.

We shall see later that this expression is very useful to evaluate the series expansion for the geopotential.

4.1. Proof of the Addition Theorem

In order to prove this theorem, we consider the vector s as fixed in space. Then, $P_l(\cos \gamma)$ is a function of the angles θ, φ with the angles θ', φ' as parameters. It may be expanded in a series:

$$P_l(\cos \gamma) = \sum_{l'=0}^{\infty} \sum_{m=-l'}^{l'} A_{l'm}(\theta', \varphi') Y_{l'm}(\theta, \varphi) \quad (45)$$

The comparison with equation 43 shows that only terms in $l' = l$ appear. To understand why this happens, one can note that, if coordinate axes are chosen so that \vec{s} is on the z axis, then γ becomes the usual polar angle between the two vectors and $P_l(\cos \gamma)$ satisfies the equation:

$$\nabla'^2 P_l(\cos \gamma) + \frac{l(l+1)}{r^2} P_l(\cos \gamma) = 0 \quad (46)$$

where ∇'^2 is the Laplacian referred to these new axes. If the axes are now rotated to the position that we originally had, $\nabla'^2 = \nabla^2$ and r is unchanged. Consequently $P_l(\cos \gamma)$ still satisfies 46; i.e., it is a spherical harmonic of order l . This means that it is a linear combination of Y_{lm} 's of that order only:

$$P_l(\cos \gamma) = \sum_{m=-l}^l A_m(\theta', \varphi') Y_{lm}(\theta, \varphi) \quad (47)$$

The coefficients $A_m(\theta', \varphi')$ are given by:

$$A_m(\theta', \varphi') = \int Y_{lm}^*(\theta, \varphi) P_l(\cos \gamma) d\Omega \quad (48)$$

We are not going into detail on this coefficient A_m , since it can be demonstrated [2] (Jackson, 1975) that it is equal to the following expression:

$$A_m(\theta', \varphi') = \frac{4\pi}{2l+1} \{ Y_{lm}^* [\theta(\gamma, \beta), \varphi(\gamma, \beta)] \}_{\gamma=0} \quad (49)$$

In the limit when $\gamma \rightarrow 0$, the angles (θ, φ) as functions of (γ, β) , go over into (θ', φ') . Comparing 49 to the expression 43, we see that they are equivalent and thus addition theorem is proved.

5. Geopotential Expansion

We now possess all necessary tools to expand the Earth's gravitational potential into a spherical harmonics' series. This potential was until now expressed in integral form (equation 11). In order to evaluate this integral, we are first going to focus on the inverse of the distance between the two vectors \mathbf{r} and \mathbf{s} . This quantity arises often in physics and is given by the following expression, in spherical coordinates:

$$\frac{1}{|\mathbf{r} - \mathbf{s}|} = \frac{1}{\sqrt{r^2 + s^2 - 2rs \cos \gamma}} \quad (50)$$

where $r \equiv |\vec{r}|$ and $s \equiv |\vec{s}|$. In the case of $r > s$, which holds for all points \mathbf{r} outside a circumscribing sphere, one has:

$$\frac{1}{|\mathbf{r} - \mathbf{s}|} = \frac{1}{r} \left(1 + \frac{s^2}{r^2} - \frac{2s}{r} \cos \gamma \right)^{-1/2} = \frac{1}{r} \sum_{n=0}^{\infty} \left(\frac{s}{r} \right)^n P_l(\cos \gamma) \quad (51)$$

with

$$\cos \gamma = \frac{r \cdot s}{rs} \quad (52)$$

and $P_l(\cos \gamma)$ is the Legendre polynomial of degree n , and γ is the angle between \mathbf{r} and \mathbf{s} . If we now substitute the result from the addition theorem from expression 44 on the expression 51, and using the longitude λ (counted positively towards the Earth) and the geocentric latitude ϕ of the point \mathbf{r} according to:

$$\begin{aligned} x &= r \cos \phi \cos \lambda \\ y &= r \cos \phi \sin \lambda \\ z &= r \sin \phi \end{aligned} \quad (53)$$

as well as the corresponding quantities λ' and ϕ' for s , one is now able to write the Earth's gravity potential in the form:

$$U = \frac{GM_{\oplus}}{r} \sum_{n=0}^{\infty} \sum_{m=0}^{\infty} \frac{R_{\oplus}^n}{r^n} P_{nm}(\sin \phi) (C_{nm} \cos(m\lambda) + S_{nm} \sin(m\lambda)) \quad (54)$$

with coefficients:

$$\begin{aligned} C_{nm} &= \frac{2 - \delta_{0m}}{M_{\oplus}} \frac{(n-m)!}{(n+m)!} \int \frac{s^n}{R_{\oplus}^n} P_{nm}(\sin \phi') \cos(m\lambda') \rho(s) d^3s \\ S_{nm} &= \frac{2 - \delta_{0m}}{M_{\oplus}} \frac{(n-m)!}{(n+m)!} \int \frac{s^n}{R_{\oplus}^n} P_{nm}(\sin \phi') \sin(m\lambda') \rho(s) d^3s \end{aligned} \quad (55)$$

which describe the dependence on the Earth's internal mass distribution $\rho(s)d^3s$. The geopotential coefficients with $m = 0$ are called **zonal coefficients**, since they describe the

part of the potential that does not depend on the longitude θ . Also, we can note that since m is the argument of $\sin(m\lambda')$, all S_{n0} vanish due to their definition, and the notation:

$$J_n = -C_{n0} \quad (56)$$

is used for the remaining zonal terms. The other coefficients are known as **tesseral** and **sectorial** coefficients, for $m < n$ and $m > n$, respectively.

5.1. The Normalized Geopotential Coefficients

Since the geopotential coefficients C_{nm} and S_{nm} cover a range of ten or more orders of magnitude, even considering a small model, the normalized coefficients \bar{C}_{nm} and \bar{S}_{nm} are given, which are defined as the following expression:

$$\begin{Bmatrix} \bar{C}_{nm} \\ \bar{S}_{nm} \end{Bmatrix} = \sqrt{\frac{(n+m)!}{(2-\delta_{0m})(2m+1)(n-m)!}} \begin{Bmatrix} C_{nm} \\ S_{nm} \end{Bmatrix} \quad (57)$$

The normalized coefficients are much more uniform in magnitude than the unnormalized coefficients, and their size is given approximately by the empirical *Kaula rule* as:

$$\bar{C}_{nm}, \bar{S}_{nm} \approx \frac{10^{-5}}{n^2} \quad (58)$$

Later in this project we are going to explore deeper these normalized coefficients. For now, making use of the expression given by 57, the acceleration due to the Earth's gravity potential may be written as:

$$\ddot{r} = \nabla \frac{GM_\oplus}{r} \sum_{n=0}^{\infty} \sum_{m=0}^n \frac{R_\oplus^n}{r^n} \bar{P}_{nm} (\sin \phi) (\bar{C}_{nm} \cos(m\lambda) + \bar{S}_{nm} \sin(m\lambda)) \quad (59)$$

where the normalized associated Legendre functions are given as:

$$\bar{P}_{nm} = \sqrt{\frac{(2-\delta_{0m})(2n+1)(n-m)!}{(n+m)!}} P_{nm} \quad (60)$$

Differently from the normalized Legendre functions P_{nm} , \bar{P}_{nm} exhibit a less pronounced variation with n and m , according to their normalized relations. We shall see later applications of these functions when exploring more properties of spherical harmonics.

6. Physical interpretation of spherical harmonics

6.1. Zonal, Sectorial and Tesseral terms

The core of this section will be the interpretation of the expression in equation 54, the result obtained for the gravitational potential of an arbitrary body. An explanation follows on how the spherical harmonics model different distributions of mass, why this is a good approximation for the gravitational potential model (and its range of validity) and finally a discussion on the relative importance of terms.

Firstly, we will dwelve into the zonal harmonics. These are harmonics that measure variations of gravity with latitude, the changes between the torrid, temperate and frigid zones of the Earth. The even degree zonal harmonics are symmetrical about the equator while the odd degree ones are asymmetrical [8].

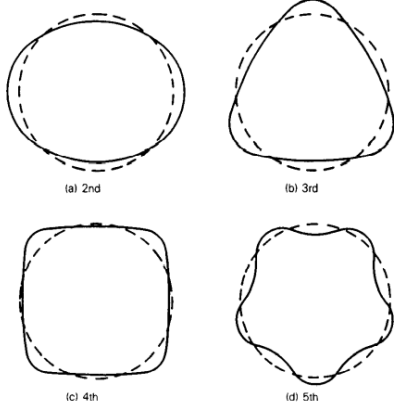


Figure 5: Form of the second to fifth zonal harmonics. The second harmonic corresponds to the Earth's flattening, the third expresses the 'pear-shape' effect, the fourth harmonic is square-shaped, the fifth has five 'petals', and so on [8].

The sections shown in this picture are slices through the poles. Since zonal harmonics measure variations of gravity with latitude you can represent them in this fashion without loss of detail. Using only the zonal terms as an infinite series, it is possible to perfectly match the gravitational potential of any solid of revolution:

$$U = \frac{\mu}{r} \left\{ 1 - \sum_{n=2}^{\infty} J_n \left(\frac{R}{r} \right)^n P_n(\sin\phi) \right\} \quad (61)$$

In this expression, worth bringing up because the J_n notation became standard, μ is the gravitational constant for the Earth, $398\,600\,km^3/s^2$, and $P_n(\sin\phi)$ is the ' n^{th} harmonic', or the Legendre polynomial of degree n and argument $\sin\phi$, where ϕ is the latitude. Note that both n and l have become standard to represent the degree of the spherical harmonic, so we will sometimes alternate between them since different authors follow different conventions.

The J_n are constant coefficients that can be evaluated up to higher and higher values of n as data from more and more satellites comes in. By combining all these harmonics one can already create a much better representation of the real geopotential, when compared to the homogeneous sphere approximation. These harmonics are termed "zonal" since the curves on a unit sphere (with center at the origin) on which $P_n(\sin\phi)$ vanishes are n parallels of latitude which divide the surface into zones (Whittaker and Watson 1990, p. 392).

When the degree, n , of the spherical harmonic is equal to the absolute value of the order, $|m|$, there are no zero crossings in latitude and the functions are referred to as sectorial (or sectoral). For the other cases, the functions checker the sphere, and they are referred to as tesseral [9].

A tesseral harmonic is so named because the curves on which they vanish are **n-m** parallels of latitude and **2m** meridians, which divide the surface of a sphere into quadrangles whose angles are right angles (Whittaker and Watson 1990, p. 392). Also worth noting that to apply the concepts of angles to the surface of a sphere we have to step into the realm of non-euclidean geometry. This is obviously outside the scope of the work but is of importance when trying to figure out how a triangle can have 3 right angles, for example in the images presented below.

In general, $\Re[Y_{nm}]$ is equal to 0 along m great circles passing through the poles, and along $n-m$ circles of equal latitude. The function changes sign each time it crosses one of these lines, as you can see below [9].

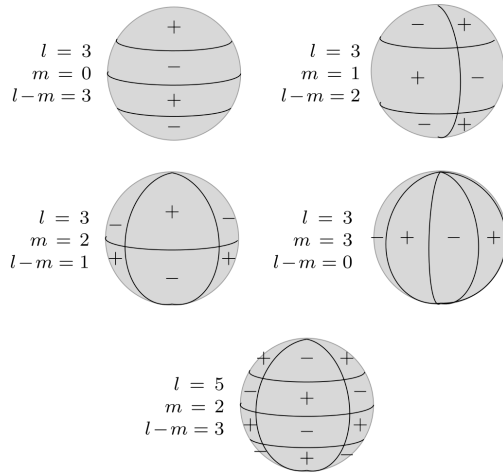


Figure 6: Schematic representation of $Y_{\ell m}$ on the unit sphere and its nodal lines.

Below follow two more representations of the different spherical harmonics. The first one, on the left, represents the positive and negative regions as dark and white zones, respectively. The image on the right, however, follows a more geometrical approach. It gives an intuitive insight into what the positive/negative regions mean in terms of gravitational potential, since the positive regions are depicted as convex, protruding outwards, and the negative regions forming a concave surface. Therefore, a positive sign means that bodies directly above that region experience greater gravitational pull. These regions can also be interpreted as zones with varying densities of mass.

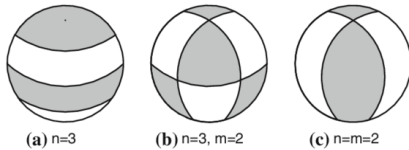


Figure 7: The 3 types of spherical harmonics. **n** indicates the degree of the harmonic, **m** the order [10].

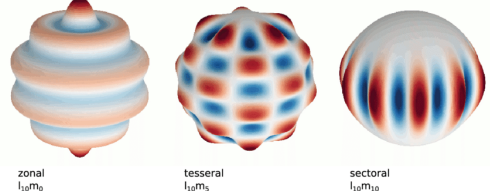


Figure 8: 3-D illustrations of zonal, tesseral, and sectoral spherical harmonic functions [11].

6.2. Spherical Harmonics' Completeness

Like it has been explained before, the spherical harmonics' functions form a complete set of orthogonal functions. This completeness implies that the expansion converges to an exact result for sufficient terms. The more spherical symmetry the original function possesses, the shorter the expansion and the fewer parameters will have to be determined [12]. The more irregular the body is, the more important the higher order terms are.

The image presented below is taken from a study that employed spherical harmonics in order to perform a surface parametrisation. The mannequin head is approximated by growing degrees of spherical harmonics. While for an approximation of the gravitational potential of the Earth, an acceptable model could be built with only two degrees of spherical harmonics (the reference ellipsoid, which we will cover later), in this case, even with 10 degrees, the result is quite poor. We can still observe appreciable improvement in results from the 40 to 60 degrees leap.

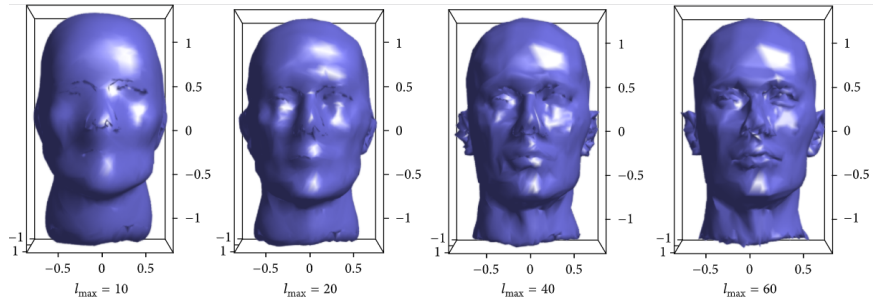


Figure 9: Original surface meshes of a mannequin approximated by spherical harmonics and meshed using the original vertex angles and face information using increasing values of l_{\max} [13].

A question that we have not yet answered in detail is the range of validity of this expression. As referred in section 5, in order to evaluate the integral in equation 11, we must find a way to compute the inverse of the distance between the two vectors \mathbf{r} and \mathbf{s} .

The inverse of the distance may be expanded in a series of Legendre polynomials. For $r > s$, which holds for all points \mathbf{r} outside a circumscribing sphere, we get the result shown previously in equation 51

Note that we imposed a condition, $r > s$, in order to develop this expansion. Therefore, it is only valid for $|\mathbf{r}|$ greater than the distance from the center of the body to the mass element furthest from it. The circumscribing sphere is also called the minimum Brillouin sphere, the smallest volume sphere with its center in the center of the body within which all mass elements of the body reside. For simplicity's sake, we assume that the body we are working with is homogeneous: its center is, therefore, the centroid and also its center of mass. Thus, the exterior gravity field does not model the dynamical environment within the Brillouin sphere, which poses a problem when performing proximity operations around asteroids and other highly irregularly shaped bodies [14].

Inside the Brillouin sphere, the convergence of the spherical harmonic series is not guaranteed. Near or at the surface of the masses, series convergence must be looked upon as

an unstable property. This means that an arbitrarily small change of the mass distribution may change convergence to divergence. Generally, divergence is thought to be more likely the more irregular the planetary body and the deeper the evaluation points are located inside the Brillouin sphere [15]. Other models, such as the polyhedral gravity field, converge anywhere around the body (even on the surface), despite coming at a higher computational cost.

6.3. Spherical Harmonics in Quantum Physics

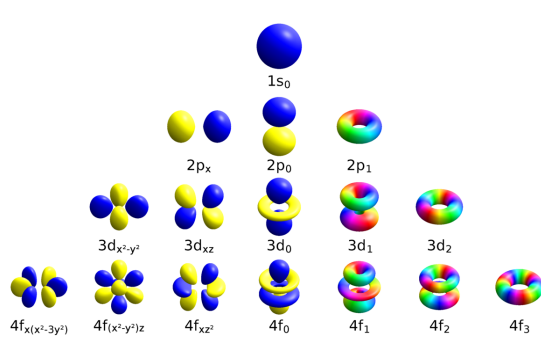
Spherical harmonics are not only fundamental in the construction of gravity models, they are also ubiquitous in atomic and molecular physics. In fact, the most common orbital descriptions are based on the solutions to the hydrogen atom, where orbitals are given by the product between a radial function and a pure spherical harmonic. Instead of building atomic orbitals out of the product of radial functions and a single spherical harmonic, linear combinations of spherical harmonics are typically used, designed so that the imaginary part of the spherical harmonics cancel out. These real orbitals are the building blocks most commonly shown in orbital visualizations. As an example, the real hydrogen-like p orbitals are given by the following [16]:

$$p_z = p_0 \quad (62)$$

$$p_x = \frac{1}{\sqrt{2}}(p_1 + p_{-1}) \quad (63)$$

$$p_y = \frac{1}{i\sqrt{2}}(p_1 - p_{-1}) \quad (64)$$

Below, a comparison between the first atomic orbitals and a table of the real spherical harmonics.



7. Shell theorem

The Shell Theorem is a theorem proposed by Isaac Newton which states that a gravitational field outside a spherical shell of mass M is the same as if that mass M was concentrated at its center (of mass). It also states that the gravitational field inside a spherical shell is 0.

7.1. Proof of Newton's Shell Theorem

Let's consider a spherical shell of mass M and radius R . In order to compute the gravitational field E we can decompose the shell into thin circular rings, each at a variable distance s from the point where we are calculating the gravitational field as seen in figure 12.

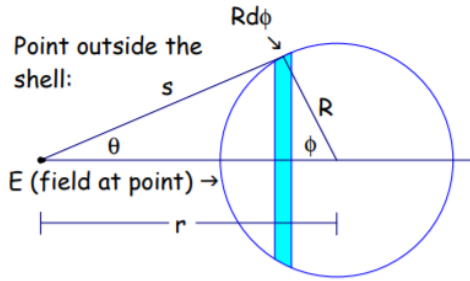


Figure 12: Shell decomposition.

[18]

The shell's density is given by $\rho = \frac{M}{4\pi R^2}$, so we can obtain the mass of each ring as follows

$$\begin{aligned} M_{ring} &= \rho A_{ring} \\ &= \rho \times 2\pi R \sin \phi \times R d\phi \\ &= \frac{1}{2} M \sin \phi d\phi \end{aligned} \tag{65}$$

As each ring's mass is at a distance s from the point, the direction of the field must point to the center of the sphere. Therefore, the field induced by each ring is

$$dE = \frac{GM \cos \theta \sin \phi d\phi}{2s^2} = -\frac{GM \cos \theta d(\cos \phi)}{2s^2} \tag{66}$$

Using the law of cosines, we can write

$$R^2 = s^2 + r^2 - 2rs \cos \theta \tag{67}$$

and

$$s^2 = R^2 + r^2 - 2Rr \cos \phi. \tag{68}$$

Consequently,

$$\cos \theta = \frac{s^2 + r^2 - R^2}{2rs} \tag{69}$$

and

$$\cos \phi = \frac{R^2 + r^2 - s^2}{2Rr}, \quad (70)$$

which gives us

$$-d(\cos \phi) = \frac{s}{Rr} ds. \quad (71)$$

Plugging in this result in equation 66 we obtain the field contribution of a thin ring,

$$dE = \frac{GM(s^2 + r^2 - R^2)}{4Rr^2 s^2} ds. \quad (72)$$

Finally, integrating this relation to obtain the total gravitational field created by the spherical shell, we get

$$E = \frac{GM}{4Rr^2} \int_{s=r-R}^{s=r+R} \frac{s^2 + r^2 - R^2}{s^2} ds = \frac{GM}{4Rr^2} \times 4R = \frac{GM}{r^2}, \quad (73)$$

which is the same result as if we had a point mass.

This important result enables us to use Newton's Universal Law of Gravitation on bigger bodies such as planets, given the assumption that they are spherical bodies. This means we can use Newton's Universal Law of Gravitation directly to obtain an equation for the gravitational field of spherical bodies:

$$\vec{F}_g = -\frac{GMm}{r^2} \vec{e}_r \iff \vec{g}(r) = -\frac{GM}{r^2} \vec{e}_r \quad (74)$$

To prove that the gravitational field inside the shell is 0, we only need to change the limits of integration for s .

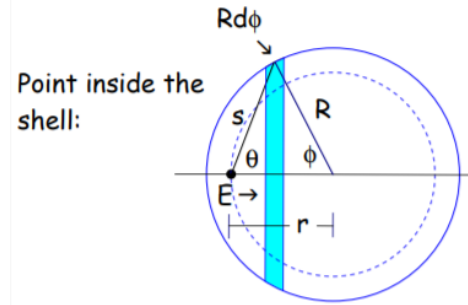


Figure 13: Calculations for the field inside a shell.

[18]

Integrating,

$$E = \frac{GM}{4Rr^2} \int_{s=R-r}^{s=R+r} \frac{s^2 + r^2 - R^2}{s^2} ds = \frac{GM}{4Rr^2} \left(s + \frac{R^2 - r^2}{s} \right) \Big|_{R-r}^{R+r} = 0 \quad (75)$$

The last step in this proof is to determine the gravitational field induced by a homogeneous spherical mass, with total mass M . The density of this mass is given by

$$\rho = \frac{3M}{4\pi R^3}, \quad (76)$$

with r being the distance from the center of the sphere to the point where the field is to be determined.

If the sphere is divided into concentric thin shells, with radius α and thickness $d\alpha$, the mass of each shell is given by

$$dM = 4\pi\alpha^2\rho d\alpha = \frac{3M\alpha^2}{R^3}d\alpha. \quad (77)$$

This way, using the first part of the Shell Theorem, the value of the gravitational field induced by one shell can be obtained as follows,

$$dE = \frac{3GM\alpha^2}{r^2R^3}d\alpha. \quad (78)$$

Thus, the total field strength for a point outside the mass (r) is

$$E = \int_0^R dE = \int_0^R \frac{3GM\alpha^2}{r^2R^3}d\alpha = \frac{GM\alpha^3}{r^2R^3} \Big|_0^R = \frac{GM}{r^2}. \quad (79)$$

For a point inside the spherical mass ($r < R$), the second part of the Shell Theorem is used, which gives

$$\begin{cases} dE = \frac{3GM\alpha^2}{r^2R^3}d\alpha, & \text{if } 0 \leq \alpha \leq r \\ 0, & \text{if } r \leq \alpha \leq R \end{cases} \quad (80)$$

From this result, the total field can be obtained integrating as follows,

$$E = \int_0^r dE = \int_0^r \frac{3GM\alpha^2}{r^2R^3}d\alpha = \frac{GMr^3}{r^2R^3} = \frac{G}{r^2} \times \text{total mass of the sphere with radius } r, \quad (81)$$

since $M_{\text{sphere with radius } r} = M \frac{r^3}{R^3}$.

8. Gauss's Law

Gauss's Law for Gravity is equivalent to Newton's Universal Law of Gravitation, but it is more practical and convenient to use. Also known as Gauss's Flux Theorem for Gravity, it can be derived from Newton's law. This result is important, as it will be used in later proofs.

8.1. Gauss's Law derivation

Newton's Universal Law of Gravitation tells us:

$$\vec{g}(r) = -\frac{GM}{r^2} \vec{e}_r, \quad (82)$$

with \vec{e}_r being the radial unit vector, r the modulus of the position vector (radial), and M the body's mass, which is assumed to be a point mass located on the origin of the frame of reference.

$g(r)$, the gravitational field in r , can be obtained by adding the contribution of all the masses in the universe (superposition principle); therefore, we integrate over all s points in space, adding the contribution of the eventual mass in s , which can be obtained using Newton's law.

$$g(r) = -G \int \rho(s) \frac{(r-s)}{|r-s|^3} d^3s, \quad (83)$$

where d^3s means $ds_x ds_y ds_z$, each one integrated from $-\infty$ to ∞ . Applying the divergence on both sides of the equation, and considering that

$$\nabla \cdot \left(\frac{r}{|r|^3} \right) = 4\pi\delta(r), \quad (84)$$

where $\delta(r)$ is the Dirac delta function, the following result is obtained:

$$\nabla \cdot g(r) = -4\pi G \int \rho(s)\delta(r-s) d^3s. \quad (85)$$

Finally, using the sifting property of Dirac's function given the fact that it is an even function, we get

$$\nabla \cdot g(r) = -4\pi G\rho(r). \quad (86)$$

This is the differential form of Gauss's Law. The integral form can be written as

$$\partial_V g \cdot dA = -4\pi GM. \quad (87)$$

This result is commonly used to calculate the intensity of Earth's gravitational field at a certain depth.

In practice, it tells us the total gravitational flux that passes through a sphere that includes the Earth (assuming it is a sphere, for this example) is $4\pi GM$; dividing this by the area of the sphere (Gaussian surface), which is $4\pi R_\oplus^2$, we get $g(r = R_\oplus) = -\frac{GM}{R_\oplus^2}$, whose absolute value is 9.81 m/s^2 , the gravitational acceleration on Earth [19]. If we divide by an arbitrary radius $r > R_\oplus$ we get $g(r)$ for any distance from the Earth's surface: $g(r) = \frac{GM}{r^2}$.

One intuitive way of formulating Gauss's Law is: "The gravitational flux that passes through any closed surface is proportional to the mass included in that surface".

8.2. Gravitational field inside the Earth for different density models

Even though considering constant density for the Earth makes many problems simpler, that is not the reality. In this section, the Earth will be considered to have different decreasing density curves and the gravitational field will be analyzed.

Considering Gauss's Law,

$$\partial_V g \cdot dA = -4\pi GM, \quad (88)$$

and noting that

$$A_{sphere} = 4\pi r^2 \iff \frac{dA}{dr} = 8\pi r \iff dA = 8\pi r dr, \quad (89)$$

we can write

$$\int_0^r g 8\pi r dr = -4\pi GM \iff 4\pi gr^2 = 4\pi GM. \quad (90)$$

We can start by setting density curves that follow an equation such as $\rho = -\alpha r^n + \rho_0$, where α is a constant, n is a parameter that we can adjust and ρ_0 is the core's density. We can also say that $\rho = \frac{M}{V} \iff dM = \rho dV$; also, for a sphere we know that $V = \frac{4}{3}\pi r^3 \iff dV = 4\pi r^2 dr$. Moreover, we can write

$$\begin{aligned} M &= \int \rho dV = \int_0^r (-\alpha r^n + \rho_0) 4\pi r^2 dr \\ &= \int_0^r \rho_0 4\pi r^2 dr - \int_0^r \alpha 4\pi r^{2+n} dr \\ &= \rho_0 4\pi \frac{r^3}{3} - \alpha 4\pi \frac{r^{3+n}}{3+n} \\ &= 4\pi r^3 \left[\frac{1}{3} \rho_0 - \alpha \frac{1}{3+n} r^n \right] \end{aligned} \quad (91)$$

To compute α for the specific case of Earth, we substitute $M = M_\oplus$ and $r = R_\oplus$ yielding

$$\begin{aligned} M_\oplus &= 4\pi R_\oplus^3 \left(\frac{1}{3} \rho_0 - \alpha \frac{1}{3+n} R_\oplus^n \right) \iff \\ \iff \alpha &= \left(\frac{M_\oplus}{4\pi R_\oplus^3} - \frac{1}{3} \rho_0 \right) \left(-\frac{3+n}{R_\oplus^n} \right) \end{aligned} \quad (92)$$

Now, replacing M in equation 90, we obtain the following expression for g :

$$\begin{aligned} 4\pi gr^2 &= 4\pi G \times 4\pi r^3 \left[\frac{1}{3} \rho_0 - \alpha \frac{1}{3+n} r^n \right] \iff \\ \iff g(r) &= 4\pi G r \left(\frac{1}{3} \rho_0 - \alpha \frac{1}{3+n} r^n \right) \end{aligned} \quad (93)$$

The value for α was calculated in order to satisfy Earth's mass given its radius as seen in equation 92.

From mere observation of the density function, we can see that it describes a linear model for $n = 1$. The following figure shows plots for some values of n :

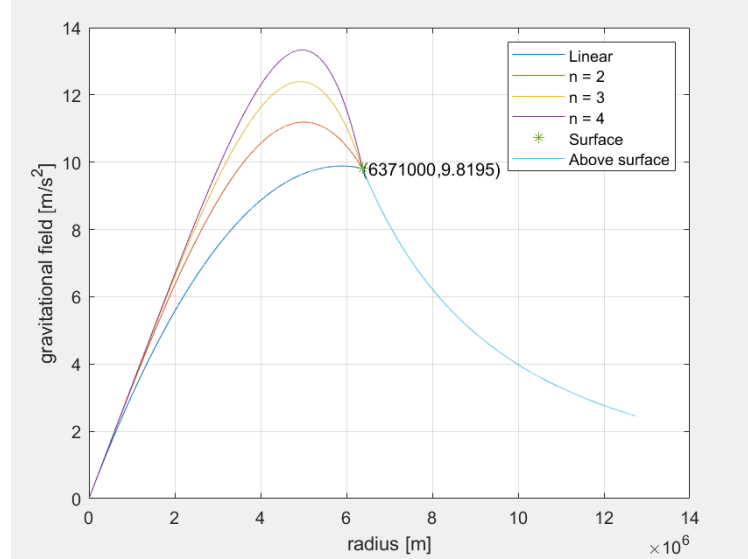


Figure 14: Solutions for the Earth's interior gravitational field using different density models.

8.3. Comparison with more realistic model

For the sake of comparison, the more accurate model for density leads to a plot as follows.

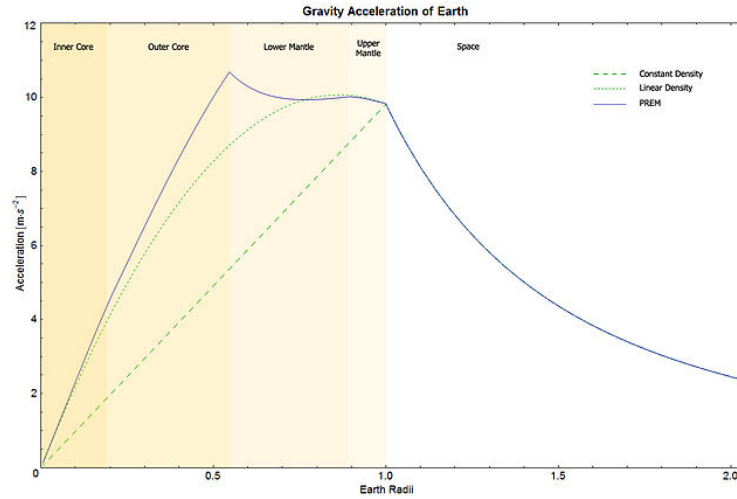


Figure 15: Plot with a more accurate solution (using PREM).

[20]

This model is based on the Preliminary Reference Earth Model (PREM), a model that describes a series of properties of our planet as functions of the radius r .

We can observe that both in the inner core and in the upper mantle, the linear model and the PREM are similar, with major differences found between the outer core and the lower mantle (which are not in solid state).

When focusing on both parts of the core, it seems that the models with higher n order are closer to the behavior predicted by the PREM.

Lastly, after reaching the surface, all models are based on a curve that behaves as a $\lambda \frac{1}{r^2}$ decay with $\lambda = GM$: Newton's Law of Gravitation.

9. Journey to the center of the Earth

One interesting problem we can consider, in which we can apply Gauss's law, is a body traveling inside the Earth, imagining there is a well going through it and passing by its center as sketched in figure 16. How long would it take for the body to go from one side to the other?

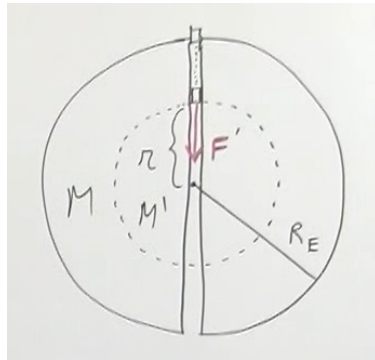


Figure 16: Sketch of the "through the Earth" hypothetical problem.

[21]

9.1. Simple harmonic motion

One way of approaching this problem is showing that the motion can be described as an harmonic oscillator, a periodic movement of a point along a line, with acceleration pointing towards a fixed point on that line and being proportional to the distance to such point (equilibrium point). In order to do that, it should be proved that the motion follows the equation $F = -kx$. There are known equations that allow us to give an answer to our question.

It is known that the force applied on a body on the surface of the Earth is given by $F = -\frac{GMm}{R_\oplus^2}$, with M being the mass of the Earth, m the mass of the body, and R_\oplus the radius of the Earth. Similarly, the force applied on a body located a distance r from the center of the Earth will be $F' = -\frac{GM'm}{r^2}$.

In order to proceed with this logic, it is assumed that the density of the Earth is constant (in reality it is not, but this approximation is satisfactory for the purpose of this problem). This way, the density of the Earth is given by $\rho = \frac{M}{V}$, and the density of the portion of the Earth limited by the sphere with radius r is $\rho' = \frac{M'}{V'}$. On the other hand, it is known that

the volume of the sphere is $V_{sphere} = \frac{4}{3}\pi r_{sphere}^3$. Thus, considering that $\rho = \rho'$ and using simple algebraic manipulation, the following relation is obtained:

$$M' = M \frac{r^3}{R_\oplus^3} \quad (94)$$

Replacing this expression for M' in the expression for F' above:

$$F' = -\left[\frac{GmM}{R_\oplus^3}\right]r \iff F' = -kx, \quad (95)$$

in other words, it is proven that the motion is a simple harmonic movement, when the stated conditions are assumed.

From the result above we can conclude that $k = \frac{GMm}{R_\oplus^3}$. Now, using the well known equations for simple harmonic motion $\omega = \sqrt{\frac{k}{m}}$ and $T = \frac{2\pi}{\omega}$, it is possible to obtain the period of the motion in study. Half of this value is going to correspond to the travel time through the Earth. Plugging in the known values of the constants, we obtain $\Delta t_{travel} = \frac{T}{2} \approx 42,2\text{min}$.

The body reaches the center of the Earth with maximum kinetic energy, which decreases throughout the second half of the movement as it totally transforms itself in potential energy on the other end of the planet. Once again, the equilibrium point of this motion is the center of the Earth.

10. Geodesy

Geodesy is "the science of accurately measuring and understanding Earth's geometric shape, orientation in space, and gravitational field" (*National Oceanic and Atmospheric Administration*, 2021).

In order to understand the analysis conducted in the next chapters, it is important to understand certain geodetic concepts that we proceed to explain.

Some things that make this subject hard to study are:

- the Earth's rotation;
- spherical harmonics are defined differently depending on the standard being used;
- the measurement of latitude and elevation;
- the anomalies are defined with respect to an ellipsoid with non-constant parameters.

10.1. Earth seen as an ellipsoid of revolution

Let a be the Earth's equatorial radius, c the polar radius, ω the angular velocity, $f = \frac{a-c}{a}$ the flattening, θ_g the geographic latitude and θ the geocentric latitude [22].

It is known that the formula that defines an ellipse in cartesian coordinates is

$$\frac{x^2}{a^2} + \frac{y^2}{a^2} + \frac{z^2}{c^2} = 1, \quad (96)$$

where the x-axis is in the equatorial plane at Greenwich (0 longitude), the y-axis is in the equatorial plane at 90° East longitude and the z-axis points along the spin axis. We can also describe the cartesian coordinates in terms of the geocentric latitude and longitude as we have previously seen in equation 53.

Plugging in the new coordinates on the ellipse's equation above and solving for r we get

$$r = \frac{1}{\sqrt{\frac{\cos^2 \theta}{a^2} + \frac{\sin^2 \theta}{c^2}}} \approx a(1 - f \sin^2 \theta). \quad (97)$$

We know from section 6 that for an ellipsoidal-shaped Earth its mass distribution is defined by the second zonal harmonic which accounts for the planet's flattening due to its rotation. This leads us to an equation that defines the potential in a non-rotating frame as

$$V = -\frac{GM_E}{r} \left[1 - J_1 \frac{a}{r} P_1(\theta) - J_2 \left(\frac{a}{r} \right)^2 P_2(\theta) \right] \quad (98)$$

By making the center of the frame coincide with the center of mass, $J_1 = 0$. Also, $P_l(x) = \frac{1}{2^l l!} \frac{d^l}{dx^l} (x^2 - 1)^l$, with $x = \sin \theta$. Therefore,

$$P_2(x) = \frac{1}{2^2 \times 2!} \frac{d^2}{dx^2} (x^2 - 1)^2 = \frac{1}{2} (3 \cos^2 \theta - 1). \quad (99)$$

This leads to the expression

$$V = -\frac{GM_{\oplus}}{r} + J_2 \frac{GM_{\oplus}a^2}{2r^3} (3 \cos^2 \theta - 1). \quad (100)$$

If compared with MacCullagh's formula, it can be concluded that $J_2 = \frac{C-A}{M_E a^2}$, with A and C being the moment of inertia about the equator and the spin axis, respectively. These values can be measured from the perturbations in the orbit of small satellites around the Earth, which leads to $J_2 = 0.001082626$ (the method used for these calculations is explained in section 15).

10.2. The reference ellipsoid

The reference ellipsoid is a mathematical figure whose surface is an equipotential of the theoretical gravity field of a symmetrical spheroidal Earth model with realistic radial variations in density.[23]

Because of their relative simplicity, reference ellipsoids are used as a preferred surface on which geodetic network computations are performed and point coordinates such as latitude, longitude, and elevation are defined.

To model the Earth, the most common reference ellipsoid used, and that used in the context of the Global Positioning System (GPS), is the one defined by WGS 84 (1984 World Geodetic System revision). This ellipsoid has a equatorial radius of $a = 6378.1370 \text{ km}$ and a polar radius of $b = 6356.7523 \text{ km}$ and is a better approximation for the shape of the earth than the sphere of mean radius $\frac{2a+b}{3} \approx 6371.0088 \text{ km}$.

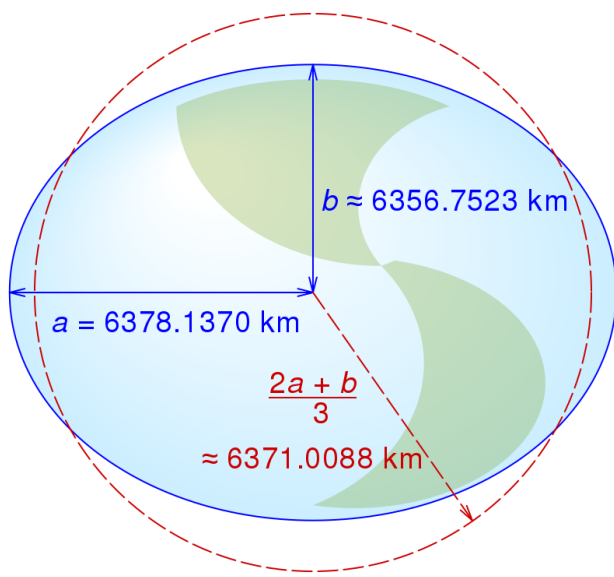


Figure 17: Equatorial (a), polar (b) and mean Earth radii as defined in the 1984 World Geodetic System revision (not to scale)

10.3. The geoid

According to Gauss, who first described it, it is the "mathematical figure of the Earth", a smooth but irregular surface whose shape results from the uneven distribution of mass within and on the surface of Earth.[24]

The geoid, defined by Earth's gravity field, is a surface of equal gravitational potential and by definition of potential, the force of gravity acts everywhere perpendicular to its surface. In other words, it follows a hypothetical ocean surface at rest (in the absence of tides and currents).

The lateral variations in density within the Earth result in deviations of the geoid from the theoretical ellipsoid.[23] The surface of the geoid is higher than the reference ellipsoid (section 10.2) wherever there is a positive gravity anomaly (mass excess) and lower than the reference ellipsoid wherever there is a negative gravity anomaly (mass deficit).

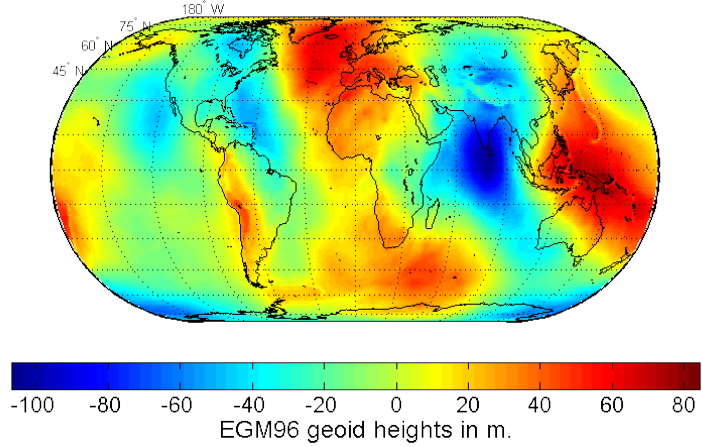


Figure 18: A view of the Earth’s geoid, as provided by EGM96

10.4. Undulation

Undulation of the geoid is the height of the geoid relative to a given ellipsoid of reference.

The undulation is not standardized, as different countries use different mean sea levels as reference (the mean sea level corresponds to the height of the geoid over the ocean), but most commonly refers to the EGM96 (Earth Gravitational Model defined in 1996) geoid (figure 18). This particular geoid model is obtained by spherical harmonics coefficients of degree and order up to 360 (which in total means we have more than 130000 coefficients).

In maps and common use the height over the mean sea level (such as orthometric height) is used to indicate the height of elevations. The orthometric height is, therefore, the distance between the surface topography and the geoid, as measured perpendicularly to the surface of the reference ellipsoid. It is represented as H in figure 19.

In contrast the ellipsoidal height results from the GPS system and similar GNSS (Global Navigation Satellite Systems). The ellipsoidal height is, therefore, the distance between the surface topography and the reference ellipsoid, as measured perpendicularly to the surface of the latter. It is represented as h in figure 19.

The geoid height is the distance between the reference ellipsoid and the geoid, as measured perpendicularly to the surface of the reference ellipsoid. It is represented as N in figure 19. This is the height that figure 18 and every other representation of the geoid henceforth refer to.

The relationship between these heights is:

$$H = h - N \quad (101)$$

and can be seen in figure 19.

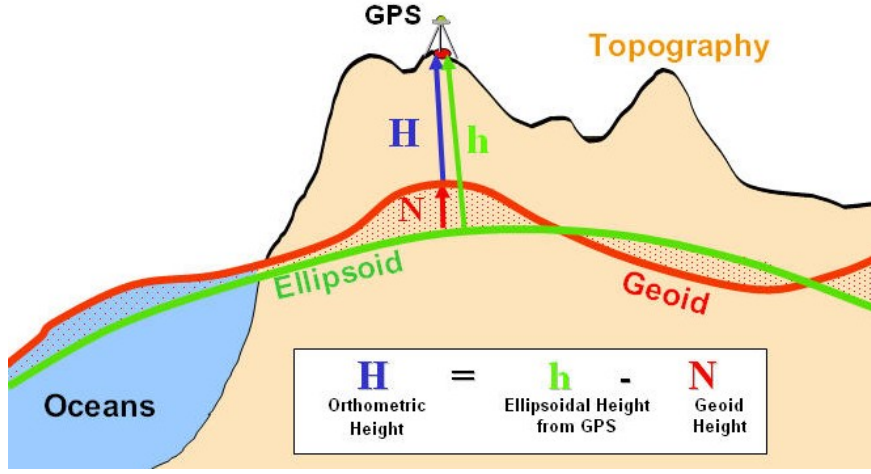


Figure 19: Schematic diagram showing geoid, ellipsoid and topography.

11. Method of Least Squares

In this section, the Least Squares Method for matrices is going to be introduced, since it is going to be useful for the following ones.

Suppose that the solution for $\mathbf{Ax} = \mathbf{b}$ is needed. This solution exists only if $\mathbf{b} \in \text{Col}(\mathbf{A})$. In the case where $\mathbf{b} \notin \text{Col}(\mathbf{A})$ there is no exact solution for \mathbf{x} , so the best approach is to find an approximate solution $\hat{\mathbf{x}}$ that makes $\mathbf{A}\hat{\mathbf{x}}$ as close to \mathbf{b} as possible. In this case, the best approximate solution is called the Least Squares solution.

Let \mathbf{A} be an $m \times n$ matrix and let \mathbf{b} be a vector in \mathbf{R}^m . A Least Squares solution of the matrix equation $\mathbf{Ax} = \mathbf{b}$ is a vector $\hat{\mathbf{x}}$ in \mathbf{R}^n such that

$$\text{dist}(\mathbf{b}, \mathbf{A}\hat{\mathbf{x}}) \leq \text{dist}(\mathbf{b}, \mathbf{Ax}) \quad (102)$$

for all other vectors \mathbf{x} in \mathbf{R}^n , with $\text{dist}(\mathbf{b}, \mathbf{A}\hat{\mathbf{x}}) = \|\mathbf{b} - \mathbf{A}\hat{\mathbf{x}}\|$

Therefore a Least Squares solution minimizes the sum of the squares of the differences between the entries of $\mathbf{A}\hat{\mathbf{x}}$ and \mathbf{b} . Using geometry, as seen in figure 20, simplifies solving this problem. Consider a plane of the $\text{Col}(\mathbf{A})$ and a vector \mathbf{b} that is not on the column space; the closest vector of the form $\mathbf{A}\hat{\mathbf{x}}$ to \mathbf{b} is the orthogonal projection of \mathbf{b} onto $\text{Col}(\mathbf{A})$, getting $\mathbf{b} = \mathbf{b}_{//} + \mathbf{b}_{\perp}$, where $\mathbf{b}_{//} \in \text{Col}(\mathbf{A})$ and $\mathbf{b}_{\perp} \perp \text{Col}(\mathbf{A})$.

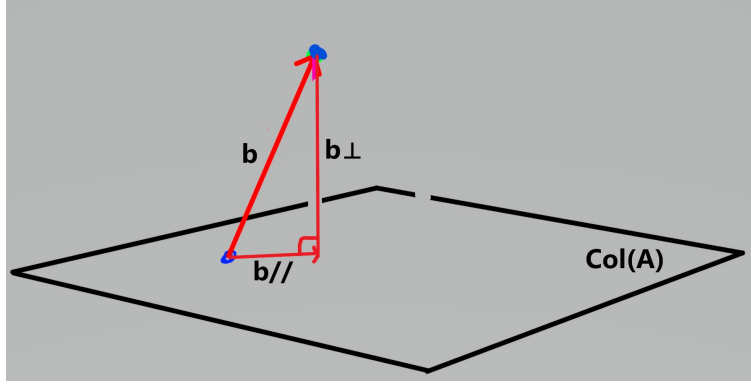


Figure 20: Column Space of A and vector b .

Note that, if $\mathbf{A} = (\mathbf{a}_1 \dots \mathbf{a}_m)$, where \mathbf{a}_i are the columns of \mathbf{A} ,

$$\mathbf{A}^T \mathbf{b}_\perp = \begin{bmatrix} \mathbf{a}_1^T \\ \vdots \\ \mathbf{a}_m^T \end{bmatrix} \mathbf{b}_\perp = \begin{bmatrix} \langle \mathbf{a}_1, \mathbf{b}_\perp \rangle \\ \vdots \\ \langle \mathbf{a}_m, \mathbf{b}_\perp \rangle \end{bmatrix} = \mathbf{0}. \quad (103)$$

Now instead of solving $\mathbf{Ax} = \mathbf{b}$ we will solve $\mathbf{Ax} = \mathbf{b}_{//}$, where $\hat{\mathbf{x}}$ minimizes $\|\mathbf{b} - \mathbf{Ax}\|$,

$$\mathbf{A}\hat{\mathbf{x}} = \mathbf{b}_{//} = \mathbf{b} - \mathbf{b}_\perp \quad (104)$$

multiplying both sides by \mathbf{A}^T we get,

$$\mathbf{A}^T \mathbf{A}\hat{\mathbf{x}} = \mathbf{A}^T \mathbf{b} - \mathbf{A}^T \mathbf{b}_\perp \quad (105)$$

but as mentioned before $\mathbf{A}^T \mathbf{b}_\perp = \mathbf{0}$, so

$$\mathbf{A}^T \mathbf{A}\hat{\mathbf{x}} = \mathbf{A}^T \mathbf{b}. \quad (106)$$

This equation represents the Least Square solution, then solving for $\hat{\mathbf{x}}$,

$$\hat{\mathbf{x}} = (\mathbf{A}^T \mathbf{A})^{-1} \mathbf{A}^T \mathbf{b} \quad (107)$$

If $\det(\mathbf{A}^T \mathbf{A}) = 0$, then there is no inverse, therefore the Moore–Penrose inverse should be used.

12. Program

For better understanding of the physical interpretation of this subject and data analysis, we developed a program in python. The program is capable of calculating and representing spherical harmonics, represent a body using spherical harmonics and calculate gravitational potential and some characteristics of the Earth's geoid.

12.1. Representing a body's surface using spherical harmonics

In this section, we explain how to represent a body using spherical harmonics, comment the results and present the conclusions.

To do this, we need some data related with the original body, specifically the geometric body vertices and faces. NASA website has several celestial bodies with this exact data, that was obtained from radars in satellites. Hence, from this website we got the data from one asteroid which comes in a file ".OBJ", as seen in figure 21, that contains thousands of vertices and faces that form a triangular mesh of the asteroid. The lines that start with a "v" represent a vertex and the next three columns are the position (x,y,z) of that vertex (these measures are not in the original scale); the lines that start with a "f" represent faces and the next three columns have the indices of the three vertices that form that face.

v -0.000000	0.000000	0.190623	f 881	1364	80
v 0.040602	0.000000	0.191238	f 1365	743	202
v 0.020562	0.035656	0.194235	f 876	1365	202
v -0.019333	0.033461	0.181428	f 816	1366	1145
v -0.038331	0.000000	0.180872	f 841	1366	816
v -0.020356	-0.035255	0.191524	f 603	119	1367
v 0.020577	-0.035615	0.193066	f 1367	119	694
v 0.077578	0.000000	0.174022	f 324	1368	834
v 0.066060	0.038161	0.171579	f 521	1368	324

(a) Vertices Sample (b) Faces Sample

Figure 21: Sample of .OBJ data file

Our goal is to get the spherical harmonics coefficients that best fit this body, so we can have an accurate representation of it, given a max degree l_{max} . In order to accomplish this, we used the method described in the following paragraphs.

From the data file, for each vertex we obtained θ , the polar angle that goes from 0 to π , ϕ , the azimuth angle that goes from $-\pi$ to π , and $f(\theta, \phi)$, the distance between the vertex and the center (origin), using the following equations:

$$f(\theta, \phi) = \sqrt{x^2 + y^2 + z^2}, \quad (108)$$

$$\theta = \arccos\left(\frac{z}{f(\theta, \phi)}\right), \quad (109)$$

$$\phi = \text{atan}2(y, x). \quad (110)$$

For some surfaces represented by a function $f(\theta, \phi)$, an infinite series of spherical harmonic basis functions can be used to represent it as

$$f(\theta, \phi) \simeq \sum_{l=0}^{l_{max}} \sum_{m=-l}^{m=l} a_{lm} Y_{lm}(\theta, \phi), \quad (111)$$

where θ and ϕ are the polar and azimuth angles in a spherical coordinate system as mentioned before. The spherical harmonic functions are defined by $Y_{lm}(\theta, \phi)$, with degree l and order m , and a_{lm} are the weighting coefficients for Y_l^m .

In this case, to calculate the spherical harmonics function $Y_{lm}(\theta, \phi)$ for $m > 0$ we used an orthonormal normalization meaning that

$$Y_{lm}(\theta, \phi) = \sqrt{\frac{2l+1}{4\pi} \frac{(l-m)!}{(l+m)!}} P_l^m(\cos(\theta)) e^{im\phi}, \quad (34 \text{ revisited})$$

where $P_l^m(x)$ are the associated Legendre polynomials,

$$P_l^m(x) = (-1)^m (1-x^2)^{\frac{m}{2}} \frac{d^m}{dx^m} P_l(x), \quad (29 \text{ revisited})$$

$$P_l(x) = \frac{1}{2^l l!} \frac{d^l}{dx^l} (x^2 - 1)^l, \quad (28 \text{ revisited})$$

and for $m < 0$,

$$Y_{l,-|m|}(\theta, \phi) = (-1)^m Y_{l|m|}^*(\theta, \phi), \quad (35 \text{ revisited})$$

where $Y_{l|m|}^*$ is the conjugate of $Y_{l|m|}$.

The function 111 may be solved for a_{lm} to calculate the weighting coefficient for each basis function, using the inverse transform,

$$a_{lm} = \int_{-\pi}^{\pi} \int_0^{\pi} f(\theta, \phi) Y_{l|m|}^*(\theta, \phi) \sin(\theta) d\theta d\phi. \quad (112)$$

This equation is often impossible to solve, so we write function 111 as a series of linear equations in matrix form,

$$\begin{bmatrix} y_{1,1} & \dots & y_{1,k} \\ \vdots & \ddots & \vdots \\ y_{n,1} & \dots & y_{n,k} \end{bmatrix} \begin{bmatrix} a_1 \\ \vdots \\ a_k \end{bmatrix} = \begin{bmatrix} f_1 \\ \vdots \\ f_n \end{bmatrix} \quad (113)$$

where the basis matrix inputs $y_{i,j} = \text{Real}(Y_{lm}(\theta_i, \phi_i))$, $j = l^2 + l + m + 1$, $k = (l_{max} + 1)^2$, $f_i = f(\theta_i, \phi_i)$ for $1 \leq i \leq n$ and n is the number of vertices. For each j corresponds an unique pair of (l,m) .

Using the Least Square Method, we can solve the matrix equation 113 and get the coefficients a_{lm} . Now with these coefficients and the same angles θ and ϕ we can do a surface parameterization by obtaining the new $\hat{f}(\theta, \phi)$ with the expression in 111. With these values, we now have the new vertices obtained by spherical harmonics in spherical coordinates, but we need them in Cartesian coordinates so we apply the following equations to each vertex:

$$x = \hat{f}(\theta, \phi) \sin(\theta) \cos(\phi), \quad (114)$$

$$y = \hat{f}(\theta, \phi) \sin(\theta) \sin(\phi), \quad (115)$$

$$z = \hat{f}(\theta, \phi) \cos(\theta). \quad (116)$$

At this point, we have the same data from file ".OBJ" but with the new vertices, and now we can compare these with the original vertices for several l_{max} as seen in figures 22 and 23. By observation, we can clearly see that the bigger the l_{max} the more accurate representation of the original body we obtain, at the cost of a bigger execution time of the program, hence as $l_{max} \rightarrow \infty$ the spherical harmonic representation becomes an exact description of the surface.

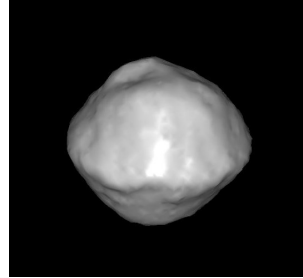


Figure 22: Original

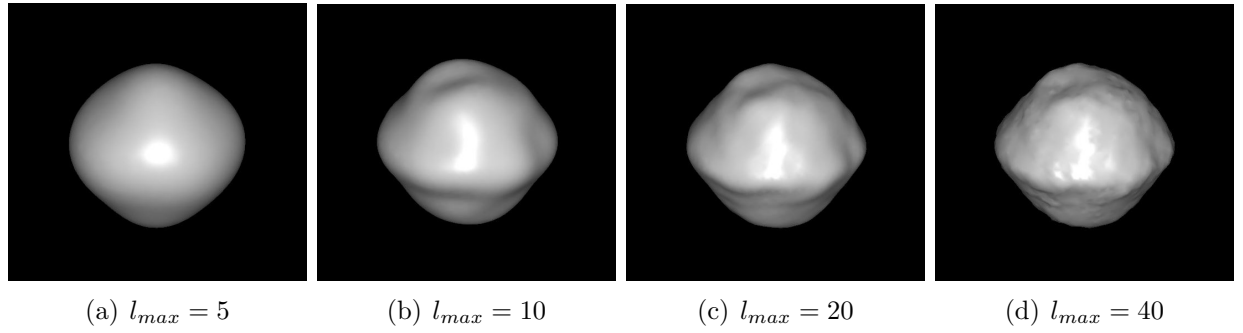


Figure 23: Spherical Harmonics Approximation

This approximation using spherical harmonics may be useful in several situations, for instance if the radar that analyses the celestial body for any reason can't fully characterize its shape. That means that there would be a hole in the triangular mesh representation, but using this method we could approximate how the body would look like in that hole, getting the complete mesh.

Another use of this method is to calculate an approximation of the gravitational potential of the body. For this we would have to assume that the celestial body has homogeneous

composition, because then the geometric shape of the body could be linearly correlated with its mass distribution.

The weighting coefficients a_{lm} are the ones responsible for the shape of the body, therefore they would also be responsible for the mass distribution, allowing us to calculate the gravitational potential as we are going to do in the following sections.

12.2. Calculating Gravitational Potential and some characteristics of the Earth's geoid

In this section, we explain how we calculated the Gravitational Potential and some characteristics of the Geoid of the Earth, using spherical harmonics.

Firstly, we need to understand the concept of EGM, already mentioned in section 10.4. The Earth Gravitational Models (EGM) are a series of geopotential models of the Earth published by the National Geospatial-Intelligence Agency (NGA). These models are used as the geoid reference in the World Geodetic System (WGS), that is a standard for use in cartography, geodesy and satellite navigation. The NGA provides the EGM models in two formats, as the series of numerical coefficients to the spherical harmonics, C_{lm} and S_{lm} , which define the model, or the geoid height at each coordinate.

In this case, we obtained the EGM96 file from the USNA (United States Naval Academy) website, containing the data referred to the spherical harmonics coefficients with max degree and order, l and m , up until 360. This data is the result of a collaboration of several agencies, with data archives being obtained for many years.

In figure 24, a sample of this file is presented. The first two columns correspond to the degree l and order m , respectively; the third and fourth columns correspond to the 4π normalized spherical harmonics coefficients, \bar{C}_{lm} and \bar{S}_{lm} ; the last two columns are the uncertainties of the two coefficients, that weren't used.

2	0	-0.484165371736E-03	0.000000000000E+00	0.35610635E-10	0.00000000E+00
2	1	-0.186987635955E-09	0.119528012031E-08	0.10000000E-29	0.10000000E-29
2	2	0.243914352398E-05	-0.140016683654E-05	0.53739154E-10	0.54353269E-10
3	0	0.957254173792E-06	0.000000000000E+00	0.18094237E-10	0.00000000E+00
3	1	0.202998882184E-05	0.248513158716E-06	0.13965165E-09	0.13645882E-09
3	2	0.904627768605E-06	-0.619025944205E-06	0.10962329E-09	0.11182866E-09
3	3	0.721072657057E-06	0.141435626958E-05	0.95156281E-10	0.93285090E-10
4	0	0.539873863789E-06	0.000000000000E+00	0.10423678E-09	0.00000000E+00
4	1	-0.536321616971E-06	-0.473440265853E-06	0.85674404E-10	0.82408489E-10

Figure 24: EGM96 data file sample.

For the following calculations, we considered that θ , the polar angle, goes from $-\frac{\pi}{2}$ to $\frac{\pi}{2}$ and ϕ , the azimuth angle, goes from $-\pi$ to π .

To calculate the gravitational potential field, $U(r, \theta, \phi)$, as a function of distance to the center r , polar angle θ and azimuth angle ϕ , we used the following formula (equivalent to equation 54),

$$U(r, \theta, \phi) = -\frac{GM_{\oplus}}{r} \left(1 + \sum_{l=2}^{\infty} \sum_{m=0}^l \frac{R_{\oplus}^l}{r^l} P_{lm}(\sin \theta) (C_{lm} \cos(m\phi) + S_{lm} \sin(m\phi)) \right), \quad (117)$$

where C_{lm} and S_{lm} are the unnormalized spherical harmonics coefficients, GM_{\oplus} is the standard gravitational parameter of the Earth, R_{\oplus} is the Earth's radius, $r > R_{\oplus}$, and $P_{lm}(x)$ are the associated Legendre polynomials,

$$P_{lm}(x) = (1 - x^2)^{\frac{m}{2}} \frac{d^m}{dx^m} P_l(x), \quad (118)$$

A change of R_{\oplus} or GM_{\oplus} , affects the geopotential coefficients C_{lm} and S_{lm} . Therefore, we must apply the R_{\oplus} and GM_{\oplus} that correspond to the coefficients C_{lm} and S_{lm} , and in this case we have: $R_{\oplus} = 6378.1363$ km; $GM_{\oplus} = 398600.4405$ km³s⁻².

The unnormalized coefficients C_{lm} and S_{lm} cover a range of ten or more orders of magnitude, and that is why in the EGM96 the coefficients are 4π normalized, because they are much more uniform. Since, we only have 4π normalized coefficients \bar{C}_{lm} and \bar{S}_{lm} , we need to normalize the expression 117, using 4π normalization. Doing so we obtain,

$$\begin{Bmatrix} \bar{C}_{lm} \\ \bar{S}_{lm} \end{Bmatrix} = \sqrt{\frac{(l+m)!}{(2-\delta_{0m})(2l+1)(l-m)!}} \begin{Bmatrix} C_{lm} \\ S_{lm} \end{Bmatrix} \quad (57 \text{ revisited})$$

$$\bar{P}_{lm} = \sqrt{\frac{(2-\delta_{0m})(2l+1)(l-m)!}{(l+m)!}} P_{lm} \quad (60 \text{ revisited})$$

and finally,

$$U(r, \theta, \phi) = -\frac{GM_{\oplus}}{r} \left(1 + \sum_{l=2}^{\infty} \sum_{m=0}^l \frac{R_{\oplus}^l}{r^l} \bar{P}_{lm}(\sin \theta) (\bar{C}_{lm} \cos(m\phi) + \bar{S}_{lm} \sin(m\phi)) \right) \quad (119)$$

To calculate the geoid height N that generates the map in figure 30, we used an approximated method that consists in the following equation,

$$N = \frac{R_{\oplus}^2}{GM_{\oplus}} (U_{zonal}(R_{\oplus}, \theta, \phi) - U(R_{\oplus}, \theta, \phi)), \quad (120)$$

where $U(R_{\oplus}, \theta, \phi)$ is the gravitational potential using all coefficients and $U_{zonal}(R_{\oplus}, \theta, \phi)$ is the gravitational potential using only the zonal coefficients.

In practice, we are calculating the potential without the zonal terms, specifically without J_2 that overwhelms all the other terms and corresponds to the ellipsoid. Therefore, we get an approximation of the difference between the other coefficients and the ellipsoid that corresponds to the geoid height.

13. Earth's geoid analysis with computational program

In this section we will analyse the results obtained by our program, taking a geoid-oriented approach. At first we will see the Earth and its potential represented through all its spherical harmonics coefficients and then layer by layer, we will remove the most dominant terms to see what the rest of the coefficients have to show.

13.1. Representing the geoid from known spherical harmonics coefficients

One of the goals of our program was to represent the geoid using the coefficients available to us in "Satellite Orbits", by Montenbruck and Gill[1].

These coefficients in particular express the potential of the earth (section 10.3). The geoid can, therefore, be represented if we use these coefficients as detailed in section 12.2.

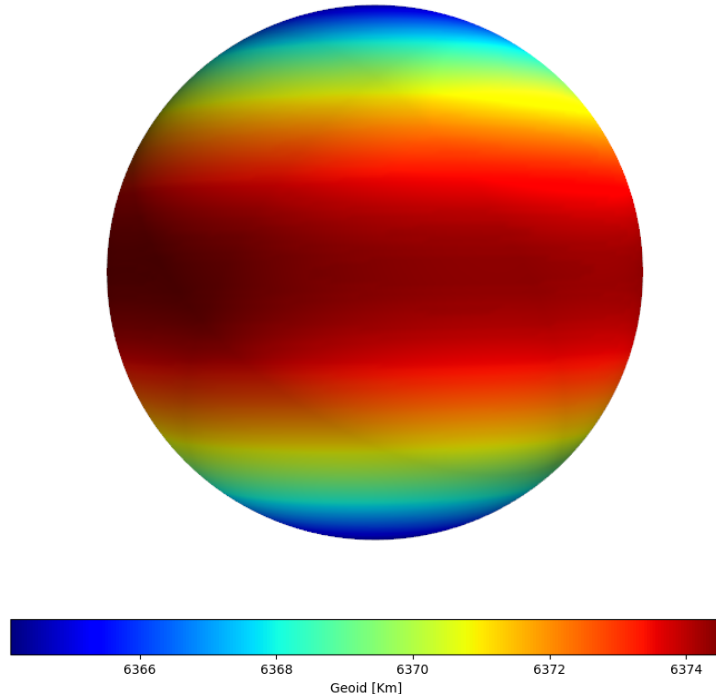


Figure 25: The geoid represented from all coefficients. Note that in the poles the radius is 6356 km and in the equator it is 6378 km, as was expected since the J_2 coefficient is predominant.

The colours here represent the distance from the center. For a certain point, if it is farther away from the center, it appears in red and if it is closer, it appears in blue.

Note that this measurement is **not** the geoid height.

At first glance the Earth appears to be a perfect sphere. The relatively small size of the deformation makes it almost unnoticeable if not highlighted by a generous scale.

The J_2 coefficient overwhelms all other deformations and in itself represents an ellipsoid that in the equator only exceeds the perfect sphere by 15 km in diameter. When we take into consideration that the Earth is 12 742 km in diameter (average), it becomes apparent why these deformations are very hard to see without scaling them up.

Here is an image with the deformations scaled up 100 times

$$R_{\text{shown}} = (R - 6371) * 100 + 6371 \text{ (km)}$$

(where 6371 is the mean radius), in order for us to be able to spot them:

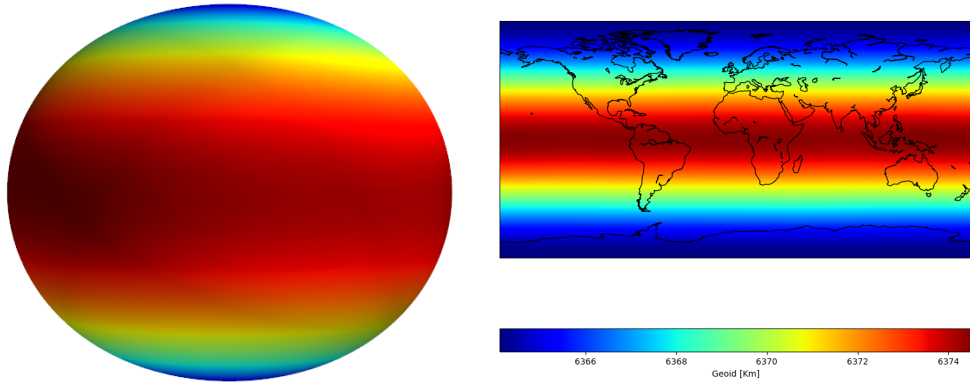


Figure 26: The geoid represented from all coefficients, but this time with scale.

With this representation it becomes clear that, if fact, the Earth is not a perfect sphere, but closer to an ellipsoid. Nonetheless, we will see in the following chapters that small deformations mean that there is no simple geometric shape that can describe it perfectly.

13.2. Individual contribution of spherical harmonics terms

If we consider the Earth to have homogeneous composition, we find that this representation matches the geometric shape of our planet. On the contrary, if we consider the Earth to be a perfect sphere, this representation matches the distribution of the density inside the planet.

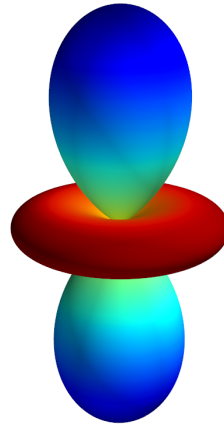


Figure 27: Real part of the spherical harmonic for $l=2$, $m=0$. (2^{nd} degree zonal harmonic)

Here we can see the spherical harmonic term for $l=2$ and $m=0$ (the spherical harmonic term corresponding to J_2). In this context, the red zones represent ones where we find the geoid surface farther away from the center than the perfect sphere and the blue ones where it is closer.

The bigger the J_2 coefficient is, the more pronounced this effect will be and greater will be the flattening of the poles, for example.

The same analysis can be drawn out for other spherical harmonics. In figure 28 we change the place of the J2 coefficient to the $l = 3$, $m = 3$ position (3^{rd} degree tesseral harmonic).

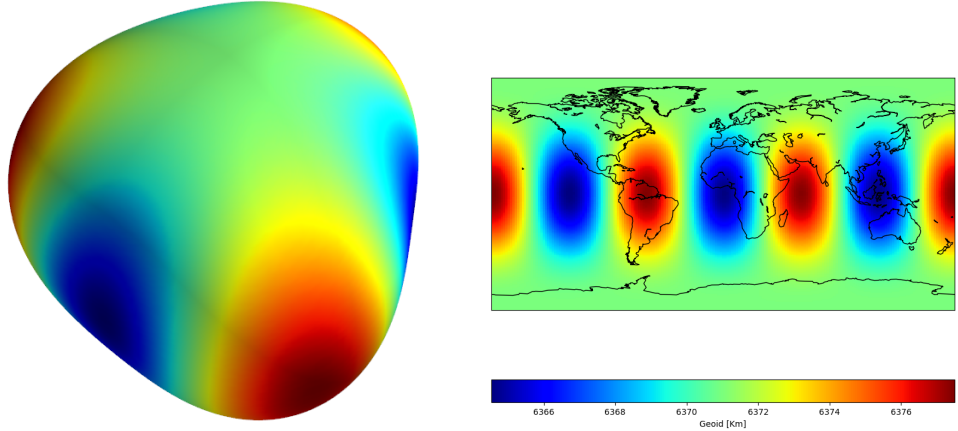


Figure 28: Geoid with the J2 coefficient of the $l = 3$ $m = 3$ position.

The predominant coefficient this time can be visualized in figure 29

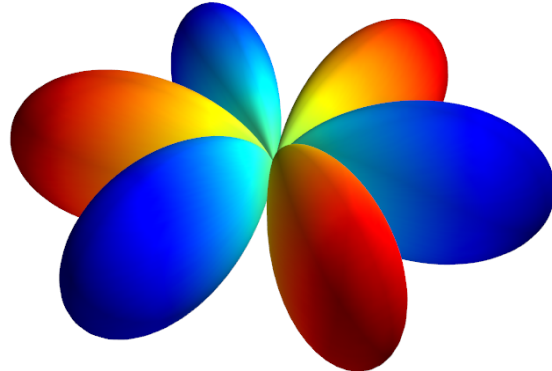


Figure 29: Real part of the spherical harmonic for $l=3$, $m =3$. (3^{rd} degree tesseral harmonic)

The colour interpretation is the same as the one done for figure 27.

13.3. Analysis of higher order terms

Just like an onion, we can peel off some spherical harmonics terms in order to better understand others.

This is what we will do next. In figure 30, we present the geoid without the overwhelming J2 coefficient in order to better observe higher order terms.

As we have seen previously, the deformations expressed in figure 26 are in the order of magnitude of the kilometers. However, the rest of the spherical harmonics terms produce

deformations in the order of magnitude of meters. It is therefore impossible for us to visualize them if the J2 coefficient is present.

Next, we display a representation of the geoid height obtained from our program. As it has been explained in section 10.4, the geoid height is the distance between the reference ellipsoid and the geoid, measured perpendicularly to the ellipsoid's surface.

In order for the deformations to be visible, they were scaled up 10000 times.

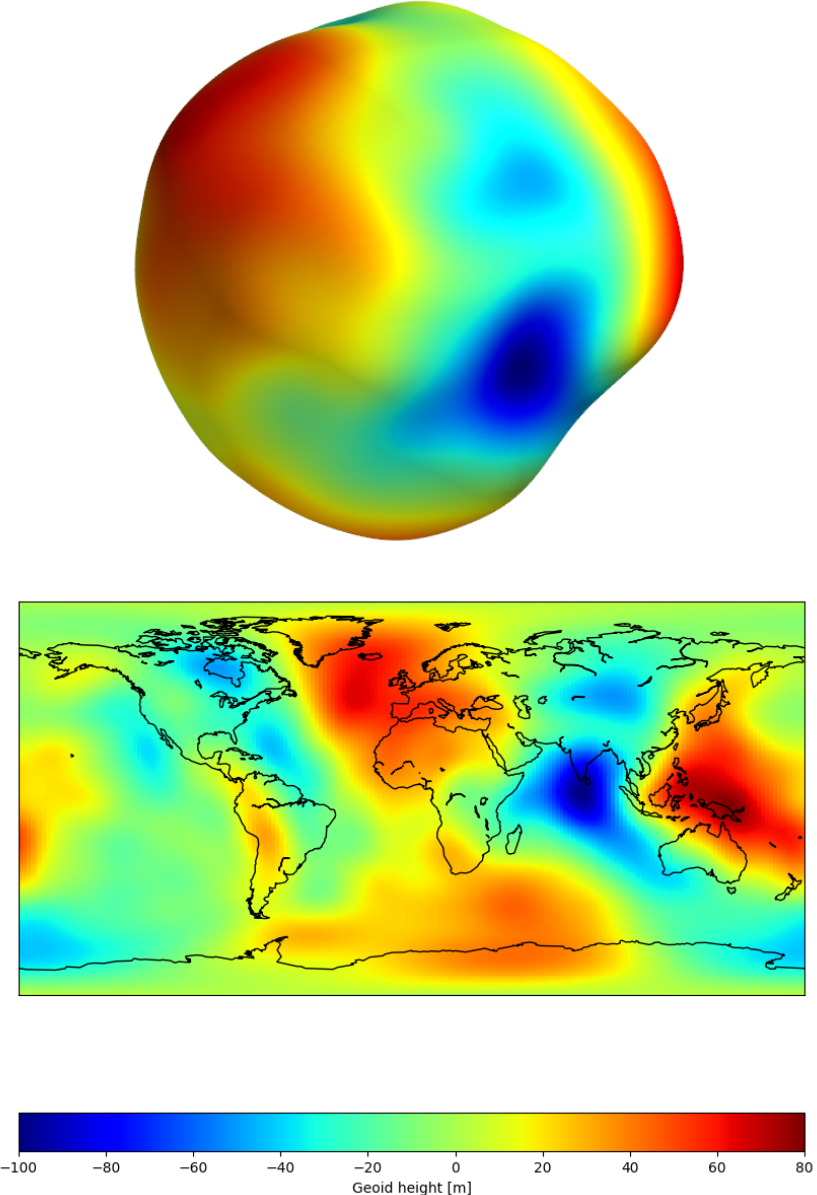


Figure 30: The geoid height. This representation removes J2 in order to be able to visualize higher order terms.

This figure (30) is remarkably similar to the figure 18, from the NASA official website[25],

which leads us to conclude that our calculations were done correctly.

14. Analysis of the Earth's gravitational potential field with computational program

14.1. Potential in a surface of constant radius outside the planet

Another way of understanding the irregularities of our planet and their influence on the gravity field, is to imagine a satellite in a circular orbit. Over time, this orbit's inclination, argument of periapsis and longitude of ascending node vary in such a way that we get a complete spherical surface around the planet.

Supposing that along all those orbits the satellite was to capture, through an array of sensors, the values of the potential field, we would have a figure such as figure 31 or 32.

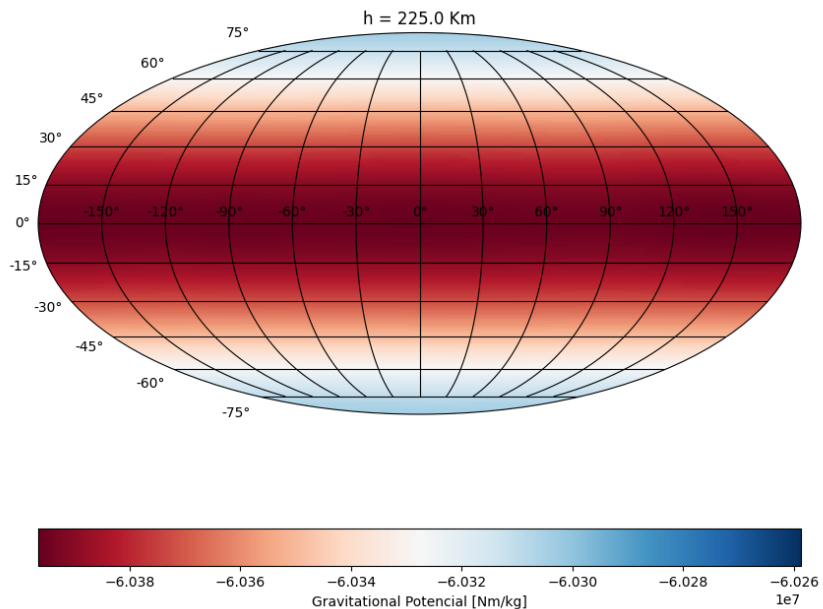


Figure 31: The potential value 225 km above the surface of the Earth

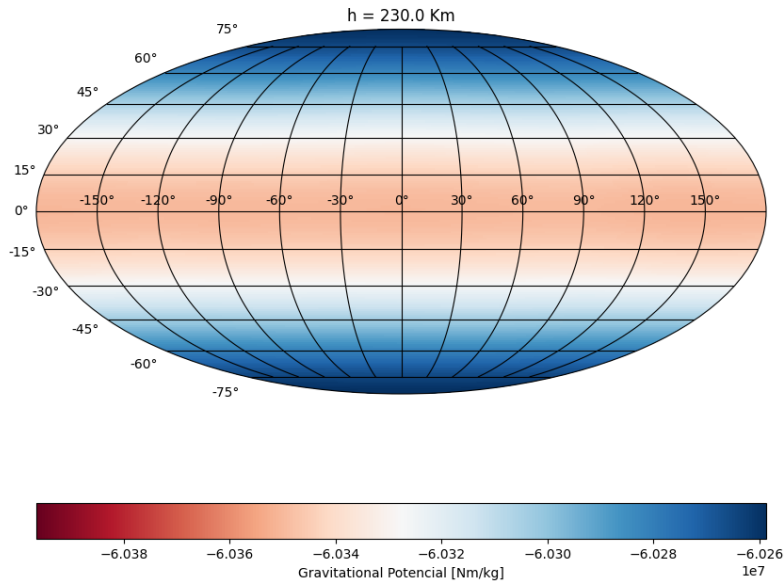


Figure 32: The potential value 230 km above the surface of the Earth

We will now do some quick calculations to verify these values. For that, we assume that the Earth is a perfect homogeneous sphere of radius 6378 km. Assuming that when $r = \infty$, the gravitational potential is zero, $\Phi = 0$, we can calculate the potential as:

$$\Phi = -\frac{GM}{r} \quad (121)$$

On the surface of the Earth, we replace r by 6378 km to get a potential of $\Phi = -6.2495e7 \text{ N m kg}^{-1}$. This puts us at a lower potential than any point in the surfaces of both of the spheres in the aforementioned figure, as was to be expected.

For 225km of altitude, we get $\Phi = -6.03666e7 \text{ N m kg}^{-1}$ at the lower end of the scale for figure 31, which indicates that the values obtained are acceptable for explanation's sake.

Both figures have been coloured with the same scale, so as to facilitate comparison between them. We can see that for a certain latitude, the potential is lower for $r = 230$ km than for $r = 225$ km. This is expected, as the probe is farther away and the radius enters as denominator in the potential formula 121.

We can also look at these figures individually and identify that the potential is higher in the poles than in the equator. This time, it is not due to a variation in the distance from center, since we are measuring in a spherical surface of constant radius.

Nonetheless, we present an explanation for this phenomenon. Because the Earth has the shape of an ellipsoid, there is a flattening of the poles and a bulge at the equator. Therefore, assuming an approximately homogeneous composition of the Earth, we can say that there is less mass near the poles and more mass near the equator.

This means that, since the mass enters the equation of the potential 121 in the numerator, a deficit in mass is accompanied by a higher potential (because of the minus sign) in the poles. By the same reasoning, an abundance of mass in the equator is accompanied by a lower potential.

It is hereby explained why, at the same distance from the center, the potential is higher in the poles and lower in the equator.

14.2. Potential in a plane that passes through the center of the Earth

Another way of looking at the potential's dependence on the radius outside the planet (the inside approach was done in section 8.2) is to cut a slice of the planet and surrounding space.

In figure 33 we analyse the potential in the equatorial plane. For this slice, we get a full plane because the angle ϕ that describes longitude goes from $-\pi$ to π rad.

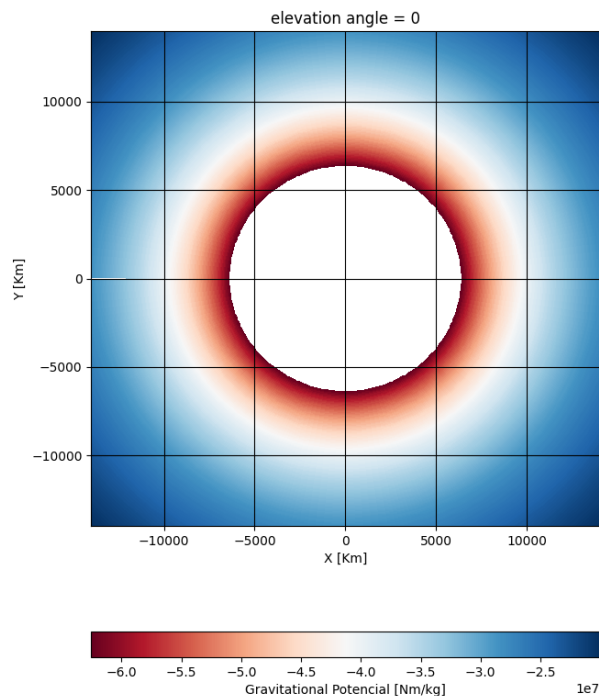


Figure 33: The potential field in the equatorial plane

Here, we only represent the potential outside the Earth, the inside being coloured in white. It is clear that the potential increases with the distance from the center. This concurs with some of the conclusions drawn out for figures 31 and 32.

In figure 34 we analyse the potential in the plane that contains the Greenwich meridian. For this, we only get a semi-plane that starts in the earth's polar axis. This is due to the fact that the angle θ that describes latitude only goes from $-\pi/2$ to $\pi/2$ rad.

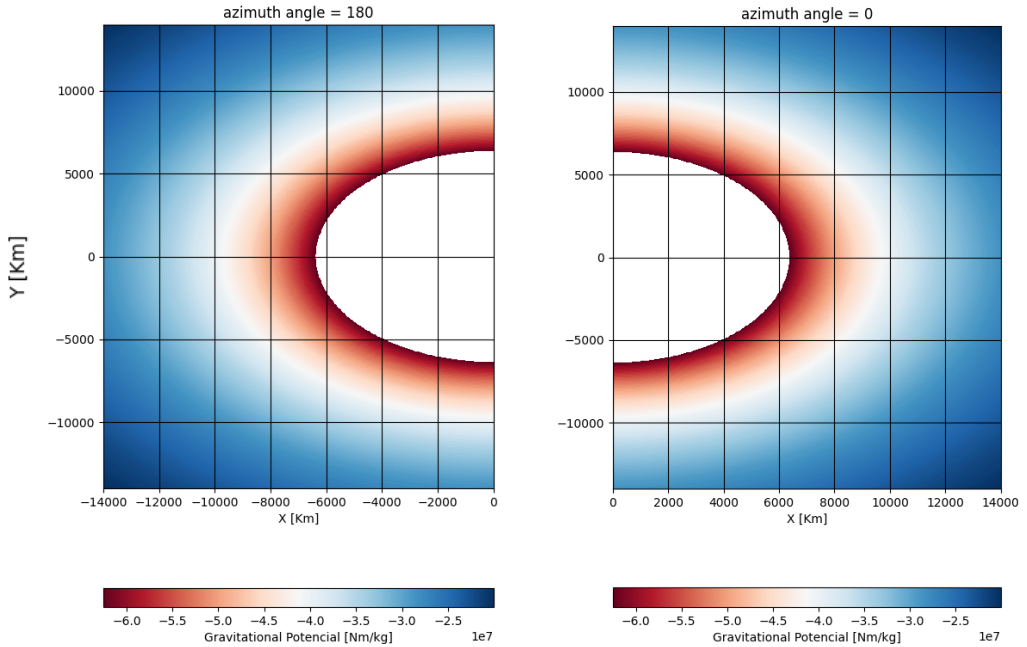


Figure 34: The potential field in the Greenwich semi-plane (right) and the one opposite to it (left).

15. GOCE space probe

A precise model of Earth's geoid is crucial for deriving accurate measurements of ocean circulation, sea-level change and terrestrial ice dynamics, all of which are affected by climate change. The improved knowledge of gravity anomalies contributed to a better understanding of Earth's interior, such as the physics and dynamics associated with volcanism and earthquakes [26].

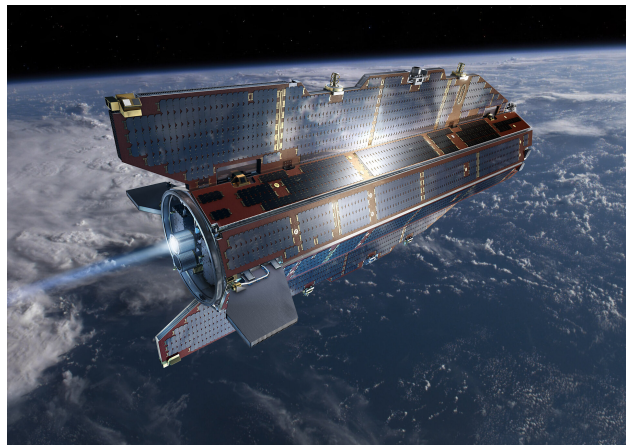


Figure 35: GOCE in orbit [27]

The Gravity Field and Steady-State Ocean Circulation Explorer (GOCE) mission has been conceived and designed to provide the most accurate, global and high-resolution map of the gravity field and its corresponding geoid surface. It combined satellite gradiometry and satellite-to-satellite high-low tracking (SST-hl) techniques that have been found to be optimum for providing the required high-quality, high-resolution static gravity field. The spacecraft was launched on 17 March 2009 and ended its mission on 11 November 2011 with a planned destructive re-entry into the atmosphere [28].

15.1. The mission

In order to deduce gravity from space, the satellite is considered a test mass in free fall in the Earth's gravitational field and from this motion the gravitational field is deduced. However, this technique comes with two limitations: satellites can be tracked from the ground only over short intervals; and satellite motion is not determined by gravitation alone but disturbed by several types of surface forces of non-gravitational origin. From these limitations, three fundamental criteria must be met:

- Uninterrupted tracking in three spatial dimensions.
- Measurement of the effect of non-gravitational forces.
- Orbital altitude as low as possible.

All three criteria can be met by exploiting the concept of satellite-to-satellite tracking in the high-low mode (SST-hl) which is employed in the GOCE mission. The high-low mode means that the tracking is performed by a satellite network above the spacecraft's orbit. The spacecraft is equipped with a GPS and GLONASS receiver and with a three-axis accelerometer. The receiver picks up the signal from twelve or more GPS and GLONASS satellites at any time, thus the orbit of the spacecraft is monitored to cm-precision without interruption and in three spatial dimensions. Even with this system, one must counteract the gravity field attenuation at altitude. The solution found by researchers was to employ Satellite Gradiometry [28]. This technique uses a pair of accelerometers to measure the difference in gravitational acceleration between two nearby points. Being a differential measurement of the gravity field, the gravity gradients are more sensitive to short wavelength features [29]. At constant instrument resolution, the actual measurement resolution depends on altitude, since the signal strength decreases rapidly with altitude. Hence, the need to fly as low as possible if high-resolution (high harmonic degree l) is sought [28]. This requires a low orbit, expected to be around 250km altitude. The orbit altitude greatly influenced the design of the probe. The satellite had a unique arrow shape and fins that helped keeping GOCE stable while travelling through the thermosphere [26]. At this operating altitude, the drag caused by the atmosphere was significant enough that it was necessary to use a means of propulsion to counter its effect, avoiding orbital decay and extending the lifespan of the mission. The engine used for the task was an ion engine. Apart from being more efficient in vacuum than a conventional chemically powered rocket engine, it is exempt from the vibrations associated with the latter. Given that the data collected was from accelerometers, this factor

was of paramount importance when choosing the means of propulsion. The satellite was maintained in this orbit by a drag-compensating ion thruster system which acts to minimise the total measured acceleration. The orbit was sun-synchronous, with an inclination of 96.5°, meaning there were polar gaps [29].

15.2. SST-hl technique

The SST-hl technique was used to derive a long-wavelength gravity field model. The GOCE satellite was equipped with two dual frequency GPS receivers which ensured uninterrupted tracking of the GOCE spacecraft. In order to recover the long-wavelength gravity field, several methods have been developed to handle SST-hl observations [30]. The main one is the Acceleration approach.

The acceleration approach is directly based on Newton's law of motion, which balances the satellite accelerations with the first-order derivatives of the gravitational potential. The theory of this approach is written as:

$$\ddot{x} - a_f = \nabla V, \quad (122)$$

where \ddot{x} denotes the satellite accelerations that are computed by numerical differentiation of the orbit data, and a_f represents the accelerations caused by the perturbing forces, V is the gravitational potential. The satellite's approach to determining the accelerations comes from the measured positions. All the parameter from Eq. (122) must be expressed in the same reference frame. In this case the IRF (Inertial Reference Frame) is chosen.

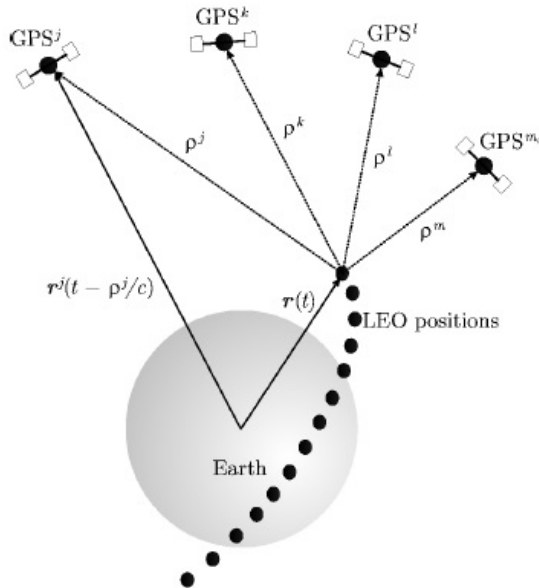


Figure 36: Kinematic Orbit Representation [31].

The SST-hl products consist of two different precise orbits: kinematic and reduced-dynamic orbit. The kinematic orbit (PKI) is a purely geometrical solution based on the

positions measured by the satellite network. The reduced-dynamic (PRD) orbit is based on the numerical integration of the equations of motion, which requires gravitational and non-gravitational force models. Therefore, it is constrained by an a priori gravity model [31]. The PKI orbit is subjected to an outlier detection. The outlier on a pre-detection phase is a kinematic position of which the difference to the PRD orbit is larger than a certain threshold. By numerical differentiation, the accelerations derived from PKI are ready for post-detection. The differences between the PKI and the estimated PRD accelerations are examined and outliers are identified if these differences exceed a given threshold. These outliers are then eliminated in order to yield a more precise solution [30].

15.3. Instrumentation

The derived model from the SST-hl observation can represent major irregularities of the Earth's gravity field. The smaller deviations that reflect the detailed structures of the Earth's gravity field are represented by higher degree and order coefficients [30].

The satellite's main payload was the Electrostatic Gravity Gradiometer (EGG). In practice, the gradiometer is built using a technique named differential accelerometry. It measures the change of the gravity acceleration between two falling proof masses which are held in a fixed position relative to each other. It contains six capacitive accelerometers arranged orthogonally [30]. The Gravity Gradiometer yields nine gravity gradient components which can be arranged in a 3x3 matrix in a Cartesian coordinate system.

$$\Gamma = \begin{bmatrix} V_{xx} & V_{xy} & V_{xz} \\ V_{yx} & V_{yy} & V_{yz} \\ V_{zx} & V_{zy} & V_{zz} \end{bmatrix} \quad (123)$$

The most frequently used and intuitive component is the vertical gravity gradient, V_{zz} , which represents the rate of change of vertical gravity (g_z) with height (z). It can be deduced by differencing the value of gravity at two points separated by a small vertical distance, l , and dividing by this distance.

$$V_{zz} = \frac{\partial g_z}{\partial z} \approx \frac{g_z(z + \frac{l}{2}) - g_z(z - \frac{l}{2})}{l} \quad (124)$$

The accelerometers are also affected by the rotation of the satellite. Each accelerometer has two sensitive axes and one less sensitive axis. These are arranged so as to provide the most accurate values of the diagonal terms V_{ii} of the tensor. The other off-diagonal terms are less well determined, so the primary output of the gradiometer measurement is the three diagonal components of the gravity tensor, after correction for rotational effects [29]. The trace of the main diagonal gradients is theoretically zero (Laplace's equation), and, in practice, it can be taken as an error measure of the main diagonal gradients. It is useful to analyse the noise behaviour of the gravity gradients. The presence of coloured noise means that values tend to be correlated with other values nearby in space or time [32]. Their correlations must be considered in the model recovery (as it will be seen later).

Being a differential measurement of the gravity field, the gravity gradients are more sensitive to short wavelength features of the field. Therefore, EGG is used to measure

high-resolution features of Earth's gravity field, while large-scale phenomena in the gravity field are obtained through analysis of GOCE's orbit as measured with a Global Navigation Satellite System receiver on the satellite.

15.4. Data Processing

The different levels of data products are:

- Level 0: Consists of the raw observations.
- Level 1a: Internal calibration.
- Level 1b: Preprocessed and calibrated observations.
- Level 2:
 - Global gravity potential modelled as harmonic coefficients.
 - Global ground-referenced gridded values of geoid heights.
 - Global ground-referenced gridded values of gravity anomalies.
- Level 3: Scientific value-added products that are derived for studies of solid-Earth physics, absolute ocean circulation, ice-sheet dynamics, geodesy and sea-level change [33].

The first step in the data analysis of both SGG and SST observations is the computation of a precise orbit. The satellite positions, taken from the SST data, enter both the SGG and orbit observation equations. A linear relation can be derived linking the SGG observations to the gravity parameters by knowing the position of the satellite. In this procedure, a-priori models have to be used to ensure the convergence to the correct solution. Linear relations can be used to compute the observation equations for the gravity gradients. For example, the SGG observations can be considered as a series in time (time-wise) or as observations at a certain location (space-wise), leading to different methods for setting up the observation equations for the gravity unknowns. Separate solutions can be derived from SGG or SST-hl observations, or combined solutions can be derived. A least-squares procedure was selected to derive the normal equations that will be solved to obtain the unknown gravity parameters. With these corrections, new reference models can be derived and the above procedure can be repeated until convergence.

The number of unknown gravity parameters (harmonic coefficients) is proportional to the square of the maximum degree L of the spherical harmonic expansion. A field of 80km resolution, for example, requires the estimation of all parameters up to degree and order 250 or $250^2 = 62500$ unknowns. Gravitational field observations (orbit and gravity gradiometer data) are required to estimate these parameters. Each observation has to be linked to the gravity parameters and thus gives rise to one observation equation. A typical figure for the number of GOCE observations is 60 million. Thus, for the estimation of 62500 parameters this would result in a linear system of 60 million equations with 62500 unknowns [28].

15.5. Least-squares adjustment

The present section was taken from (Wu, 2016).

For a linear equation system, the functional model that expresses the measurements as a function of the unknown parameters can be represented as:

$$l + v = Ax, \quad (125)$$

where l is the vector of observations, v represents observations residuals, A is the so-called design matrix and x is the vector of unknown parameters. The model that describes the accuracy and correlation of the measurements is represented by a full Variance/Covariance Matrix (VCM):

$$\sum_{ll} = \begin{bmatrix} \sigma_1^2 & \sigma_{12} & \dots & \sigma_{1n} \\ \sigma_{21} & \sigma_2^2 & \dots & \sigma_{2n} \\ \dots & \dots & \dots & \dots \\ \sigma_{n1} & \sigma_{n2} & \dots & \sigma_n^2 \end{bmatrix} \quad (126)$$

where σ_i^2 is the variance of the i^{th} measurement; σ_{ij} is the covariance between the i^{th} and j^{th} measurements. According to the rule of LS adjustment that minimize the sum of squares of weighted residuals, the solution \hat{x} is estimated by:

$$\hat{x} = (A^T P A)^{-1} A^T P l = N^{-1} W \quad (127)$$

where $P = \sum_{ll}^{-1}$ is the weight matrix, $N = A^T P A$ is the normal matrix, and $W = A^T P l$ is the right hand side of the normal equation $Nx = W$. The normal matrix N is independent of the observations since they only enter the computation of matrix W . N is only determined by the geometry of the data distribution, provided by the weight matrix.

In addition to the estimated parameters \hat{x} , the residuals \hat{v} after the adjustment have to be computed:

$$\hat{v} = A\hat{x} - l \quad (128)$$

Analysing the residuals allows us to assess the quality of the observations. They are used to calculate the posterior variance of unit weight $\hat{\sigma}_0^2$ which is a measure of the quality of the solution:

$$\hat{\sigma}_0^2 = \frac{\hat{v}^T P \hat{v}}{s - r} = \frac{l^T P l - W^T \hat{x}}{s - r} \quad (129)$$

where s, r are the number of observations and parameters, respectively. Thus the variance/covariance matrix of the \hat{x} is given by:

$$\sum_{\hat{x}\hat{x}} = \hat{\sigma}_0^2 N^{-1} \quad (130)$$

The square root of the diagonal of $\sum_{\hat{x}\hat{x}}$ gives the standard deviation of the estimated parameters of \hat{x} .

In the context of GOCE, as mentioned above, the number of observations is approximately 60 million, therefore the design matrix A , which is $s \times r$, stored in a double-precision floating format would require a memory space of more than 50 Terabyte. As an alternative, the normal matrix N is stored instead of A .

The theory presented so far does not account for the existence of systematic error in GOCE's orbit and gravity gradient observations. In this sense, the functional model has to incorporate additional parameters to absorb such systematic errors. These parameters are referred to as empirical parameters. Adding them to the model, we get:

$$l + v = A_1 x_1 + A_2 x_2 \quad (131)$$

where x_1 represents the aimed parameters along with its corresponding design matrix A_1 . x_2 and A_2 are the empirical parameter and their design matrix. By LS adjustment, we get:

$$N = [A_1 A_2]^T P [A_1 A_2] = \begin{bmatrix} N_{11} & N_{12} \\ N_{21} & N_{22} \end{bmatrix} \text{ and } W = \begin{bmatrix} W_{11} \\ W_{12} \end{bmatrix} \quad (132)$$

Since the empirical parameters are not of interest for the final solution, a Parameter Pre-elimination Technique is performed. The following equation

$$\begin{bmatrix} N_{11} & N_{12} \\ N_{21} & N_{22} \end{bmatrix} \begin{bmatrix} x_1 \\ x_2 \end{bmatrix} = \begin{bmatrix} W_{11} \\ W_{12} \end{bmatrix} \quad (133)$$

can be solved for the empirical parameter x_2 by

$$x_2 = N_{22}^{-1} W_2 - N_{22}^{-1} N_{21} x_1 \quad (134)$$

Substituting, we get

$$x_1 = (N_{11} - N_{12} N_{22}^{-1} N_{21})^{-1} (W_1 - N_{12} N_{22}^{-1} W_2) \quad (135)$$

Defining

$$N^* = N_{11} - N_{12} N_{22}^{-1} N_{21} \text{ and } W^* = W_1 - N_{12} N_{22}^{-1} W_2 \quad (136)$$

the dimension of N^* is the same as N_{11} which is the normal matrix corresponding to the parameters x_1

As mentioned, the GOCE satellite runs in a sun-synchronous orbit with an inclination of 96.5° . Consequently it cannot cover the polar regions. The absence of observations from the polar regions leads to a distortion of the zonal coefficients.

To overcome this problem, regularization is applied to stabilize the solution. Among all the methods, the Kaula regularization is mostly used. When applied, this regularization is written as:

$$\hat{x} = (A^T P A + \alpha R_{reg})^{-1} A^T P l \quad (137)$$

where α is the regularization parameter and R_{reg} represents the regularization matrix. According to Kaula's rule of thumb, the elements r_{ij} of the regularization matrix for spherical harmonic degree n are:

$$r_{ij} = \begin{cases} 10^{10}n^4 & , i = j \text{ and } m \leq m_{reg} \\ 0 & , \text{otherwise} \end{cases} \quad (138)$$

Because only the zonal and near-zonal coefficients are poorly determined, the maximum order m_{reg} can be obtained as:

$$m_{reg} = \theta_0 n, \quad (139)$$

where θ_0 is the opening angle of the gap in radians, which is approximately 6.5° for GOCE.

15.6. Model Recovery

The present section focuses on an algorithm to retrieve the wanted spherical harmonic coefficients via stochastic methods. The following algorithm is a simplification of the Monte Carlo methods.

15.6.1. Set up the functional model for each observation type

Using the LS Adjustment, the functional model for each observation type is:

- SST-hl

$$g_i = g_i^0 + \sum_{n=2}^N \sum_{m=0}^n A_{\hat{x}_{nm}} \cdot \hat{x}_{nm} \quad (140)$$

where the initial acceleration g_i^0 is computed from a normal gravity field model. The SH coefficients $\bar{C}_{00}, \bar{C}_{20}, \bar{C}_{40}, \bar{C}_{60}, \bar{C}_{80}$ of EGM2008 are used to describe the normal gravity field.

- SGG

$$V_{ij} = V_{ij}^0 + \sum_{n=2}^N \sum_{m=0}^n A_{\hat{x}_{nm}} \cdot \hat{x}_{nm} \quad (141)$$

where the initial gradients V_{ij}^0 are computed from a normal gravity field model. The SH coefficients $\bar{C}_{00}, \bar{C}_{20}, \bar{C}_{40}, \bar{C}_{60}, \bar{C}_{80}$ of EGM2008 are used to describe the normal gravity field. \hat{x}_{nm} are the unknown SH coefficients of degree n and order m . They are arranged as:

$$\hat{x}_{nm} = [\bar{C}_{nm}, \bar{S}_{nm}] = [\Delta \bar{C}_{20}, \bar{C}_{21}, \dots, \Delta \bar{C}_{40}, \dots, \bar{C}_{nn}, \bar{S}_{21}, \dots, \bar{S}_{nn}] \quad (142)$$

15.6.2. Set up the Design matrix

The next step is to set up the Design Matrix of each model. In both cases, the elements of the matrix correspond to the derivatives of the observations with respect to each coefficient:

- SST-hl

$$A_{\hat{x}_{nm}} = \frac{\partial g_i^{IRF}}{\partial \hat{x}_{nm}} \quad (143)$$

The satellite's positions are measured in the IRF (inertial reference frame)

- SGG

$$A_{\hat{x}_{nm}} = R_{LNOF}^{GRF} \frac{\partial V_{ij}^{LNOF}}{\partial \hat{x}_{nm}} (R_{LNOF}^{GRF})^T \quad (144)$$

These results are delivered in the Gradiometer Reference Frame (GRF). In order to set up the functional model, the observations (gravity gradients) and the base functions (the second order derivatives of the gravitation potential) have to be transformed into the same reference frame. It was decided to transform the base function from LNOF(local-north oriented frame) to GRF and set up the functional model in GRF. In this way, the functional model can be written as:

$$V_{ij} = R_{LNOF}^{GRF} V_{ij}^{LNOF} (R_{LNOF}^{GRF})^T \quad (145)$$

where the rotation matrix R_{LNOF}^{GRF} is computed by:

$$R_{LNOF}^{GRF} = R_{IRF}^{GRF} R_{ERF}^{IRF} R_{ERF}^{LNOF} \quad (146)$$

where ERF and IRF correspond to Earth-fixed Reference Frame and Inertial Reference Frame, respectively.

The advantage of the LNOF is that the derivatives can easily be written as:

$$\begin{aligned} \frac{\partial V_{xx}}{\partial \bar{C}_{nm}} + i \cdot \frac{\partial V_{xx}}{\partial \bar{S}_{nm}} &= \alpha [\bar{P}_{nm}''(t) - (n+1)\bar{P}_{nm}(t)] e^{i \cdot m \lambda}, \\ \frac{\partial V_{yy}}{\partial \bar{C}_{nm}} + i \cdot \frac{\partial V_{yy}}{\partial \bar{S}_{nm}} &= \alpha [\frac{\cos \theta}{\sin \theta} \bar{P}'_{nm}(t) - (n+1)\bar{P}_{nm}(t) - \frac{m^2}{\sin^2 \theta} \bar{P}_{nm}(t)] e^{i \cdot m \lambda}, \\ \frac{\partial V_{zz}}{\partial \bar{C}_{nm}} + i \cdot \frac{\partial V_{zz}}{\partial \bar{S}_{nm}} &= \alpha [(n+1)(n+2)\bar{P}_{nm}(t)] e^{i \cdot m \lambda}, \\ \frac{\partial V_{xy}}{\partial \bar{C}_{nm}} + i \cdot \frac{\partial V_{xy}}{\partial \bar{S}_{nm}} &= \alpha [\frac{m}{\sin \theta} \bar{P}'_{nm}(t) - \frac{m \cos \theta}{\sin^2 \theta} \bar{P}_{nm}(t)] e^{i \cdot (m \lambda + \frac{\pi}{2})}, \\ \frac{\partial V_{xz}}{\partial \bar{C}_{nm}} + i \cdot \frac{\partial V_{xz}}{\partial \bar{S}_{nm}} &= \alpha [(n+2)\bar{P}'_{nm}(t)] e^{i \cdot m \lambda}, \\ \frac{\partial V_{yz}}{\partial \bar{C}_{nm}} + i \cdot \frac{\partial V_{yz}}{\partial \bar{S}_{nm}} &= \alpha [\frac{m(n+2)}{\sin \theta} \bar{P}_{nm}(t)] e^{i \cdot (m \lambda + \frac{\pi}{2})}, \end{aligned}$$

$$\text{where, } \alpha = \frac{GM}{R} \cdot \frac{1}{r^2} \cdot (\frac{R}{r})^{n+1}, t = \cos \theta.$$

Figure 37: Derivatives of the Gravity Gradients with respect to the Spherical Harmonic Coefficients [30].

After the partial derivative coefficients of the six gradient components are computed in the LNOF, they are assembled into a matrix and then transformed into the GRF. For example, the coefficients $A_{\bar{C}_{20}}$ corresponding to the unknown parameter \bar{C}_{20} in the GRF are computed by:

$$\begin{bmatrix} A_{xx} & A_{xy} & A_{xz} \\ A_{yx} & A_{yy} & A_{yz} \\ A_{zx} & A_{zy} & A_{zz} \end{bmatrix} = R_{LNOF}^{GRF} \begin{bmatrix} \frac{\partial V_{xx}}{\partial \bar{C}_{20}} & \frac{\partial V_{xy}}{\partial \bar{C}_{20}} & \frac{\partial V_{xz}}{\partial \bar{C}_{20}} \\ \frac{\partial V_{yx}}{\partial \bar{C}_{20}} & \frac{\partial V_{yy}}{\partial \bar{C}_{20}} & \frac{\partial V_{yz}}{\partial \bar{C}_{20}} \\ \frac{\partial V_{zx}}{\partial \bar{C}_{20}} & \frac{\partial V_{zy}}{\partial \bar{C}_{20}} & \frac{\partial V_{zz}}{\partial \bar{C}_{20}} \end{bmatrix} (R_{LNOF}^{GRF})^T \quad (147)$$

The partial derivative coefficients for each gradient component are arranged in the same sequence as the unknown parameters to set up the design matrix.

15.6.3. Assemble the normal matrix

The model recovery requires an iteration step to consider the empirical VCM. In the first round, the normal matrix $N = A^T \sum^{-1} A$ is assembled by simplifying the VCM as a unit matrix, because the a-priori errors of the observations are unknown yet. The parameter pre-elimination technique is applied to eliminate empirical parameters from the normal equations. The full normal matrix is then inverted to derive the spherical harmonic coefficients, together with the standard deviations. The residuals are computed as an approximation of the true error of the observations. In the second round, an empirical VCM can be computed based on the residuals and used in the assembly of the normal matrix. The resulting full normal matrix is inverted again to derive the estimates of the coefficients and the formal errors which servers as the final output.

15.6.4. Data combination

To recover an accurate gravity field from GOCE observations, the SST-hl and SGG data must be spectrally combined because they are sensitive to different wavelengths of the gravity field [30]. Thus we cannot add their normal matrices directly. Therefore a weighted summation is perfomed whose coefficients are the inverse of their corresponding variance of unit weight. The same principle applies to the right hand side of the equations. One must also taken into account the regularization matrix because of the effect of the polar gaps.

$$(\frac{1}{\sigma_{sst}^2} N_{sst} + \frac{1}{\sigma_{sgg}^2} N_{sgg} + \alpha R_{reg})x = (\frac{1}{\sigma_{sst}^2} W_{sst} + \frac{1}{\sigma_{sgg}^2} W_{sgg}), \quad (148)$$

where N_{sst} , W_{sst} are the pre-processed normal equations for the SST-hl observations, N_{sgg} , W_{sgg} are the normal matrix and vector for the SGG observations, R_{reg} represents the regularization matrix. These matrices and vectors are summed with their weight factors $\frac{1}{\sigma_{sst}^2}, \frac{1}{\sigma_{sgg}^2}$, where $\sigma_{sst}^2, \sigma_{sgg}^2$ are the variances of unit weight for the SST-hl and SGG data (taken from Eq.129), and α is the regularization parameter which is computed from observations from previous missions (such as the GRACE mission) [34].

16. Conclusion

All in all, this research project gave us a powerful insight on how we can describe different mass shapes with the help of spherical harmonics expansions, and showed us that many factors play an important role on the gravity field created by a body.

Firstly, we showed that the spherical harmonics are a complete orthogonal set of functions and that they are used to expand the gravitational potential of the Earth. Also, completeness implies that such functions converge to an exact result for a big enough number of terms, meaning that the more terms the expansion has, the closer the resulting mass distribution is to the original object.

Nonetheless, the function for the potential of a body obtained from the spherical harmonics expansion does not model the real dynamic environment inside the volume of the Brillouin sphere.

Also, the Earth's density approximations for different functions led us to conclude that assuming a linear density model is relatively accurate for some regions inside our planet, in addition to being a simpler model for calculations.

It was also concluded that the higher the degree n of each given term with coefficient J_n , the faster the spherical harmonic term loses importance over distance as it varies with $\frac{1}{r^n}$, with J_2 being the last to disappear.

Furthermore, Earth is a perfect sphere when seen from far away because its irregularities are much less noticeable. Putting it in numbers, the J_2 coefficient leads to deformations in the order of kilometers, while higher order coefficients only correspond to irregularities in the order of meters.

Lastly, we learned that the spherical harmonics coefficients are obtained using statistical procedures: they are estimated from the solution of a linear system; this is a slow process and it is computationally expensive.

References

- [1] O. M. E. Gill, Satellite Orbits: Models, Methods and Applications, Springer, 2000.
- [2] J. D. Jackson, Classical Electrodynamics, Wiley, 1975.
- [3] N. Wheeler, Simplified production of Dirac delta function identities, Reed College Physics Department, 1997.
URL <https://www.reed.edu/physics/faculty/wheeler/documents/Miscellaneous%20Math/Delta%20Functions/Simplified%20Dirac%20Delta.pdf>
- [4] K. B. Howell, Ordinary Differential Equations: An Introduction to the Fundamentals, CRC Press, 2019.
URL <https://www.uah.edu/images/people/faculty/howellkb/DEText-Ch19.pdf>
- [5] W. contributors, Associated legendre polynomials.
URL https://www.wikiwand.com/en/Associated_Legendre_polynomials
- [6] S. S. M. Wong, Introductory Nuclear Physics, Wiley-VCH Verlag GmbH & Co. KGaA, 2004.
URL [http://faculty.washington.edu/bulgac/560_2014/\[Samuel_S._M._Wong\]_Introductory_Nuclear_Physics.pdf](http://faculty.washington.edu/bulgac/560_2014/[Samuel_S._M._Wong]_Introductory_Nuclear_Physics.pdf)
- [7] C. from the Physics 116C degree at the University of California (Santa Cruz), The Spherical Harmonics, 2012.
URL http://scipp.ucsc.edu/~haber/ph116C/SphericalHarmonics_12.pdf
- [8] D. King-Hele, A tapestry of orbits, Cambridge University Press, 2005.
- [9] W. contributors, Spherical harmonics.
URL https://en.wikipedia.org/wiki/Spherical_harmonics
- [10] M. Karbon, J. Böhm, D. Wijaya, H. Schuh, Atmospheric Effects on Gravity Space Missions, 2013, pp. 159–180. doi:https://doi.org/10.1007/978-3-642-36932-2_5.
- [11] M. Wieczorek, M. Meschede, Shtools: Tools for working with spherical harmonics, Geochemistry, Geophysics, Geosystems 19. doi:<https://doi.org/10.1029/2018GC007529>.
- [12] K. contributors, Spherical harmonics.
URL https://www.theochem.ru.nl/~pwormer/Knowino/knowino.org/wiki/Spherical_harmonics.html
- [13] C. R. Nortje, W. O. C. Ward, B. P. Neuman, L. Bai, Spherical harmonics for surface parametrisation and remeshing., Mathematical Problems in Engineering 2015. doi:<https://doi.org/10.1155/2015/582870>.
- [14] Y. Takahashi, D. Scheeres, Small body surface gravity fields via spherical harmonic expansions., Celestial Mechanics and Dynamical Astronomy 119 (2014) 169–206. doi:<https://doi.org/10.1007/s10569-014-9552-9>.
- [15] M. Šprlák, S.-C. Han, On the use of spherical harmonic series inside the minimum brillouin sphere: Theoretical review and evaluation by grail and lola satellite data, Earth-Science Reviews 222 (2021) 103739. doi:<https://doi.org/10.1016/j.earscirev.2021.103739>.
URL <https://www.sciencedirect.com/science/article/pii/S0012825221002403>
- [16] I. Levine, Quantum Chemistry (7th ed.), Pearson Education., 2014.
- [17] W. contributors, Atomic orbital.
URL https://en.wikipedia.org/wiki/Atomic_orbital#Orbitals_table
- [18] Unknown, Newton's shell theorem.
URL <https://www.math.ksu.edu/~dbski/writings/shell.pdf>
- [19] P. T., Gauss's law for gravity.
URL <https://physics.stackexchange.com/questions/242032/gauss-law-in-gravitation/242039>
- [20] Unknown, Preliminary reference earth model.
URL https://en.wikipedia.org/wiki/Preliminary_reference_Earth_model
- [21] M. van Biezen, Physics - mechanics: Ch 16 simple harmonic motion (16 of 19) time=? for trip through earth.
URL <https://www.youtube.com/watch?v=ZaNGgkCf1J0>

- [22] D. T. Sandwell, The gravity field of the earth - part 1.
URL https://topex.ucsd.edu/geodynamics/14gravity1_1.pdf
- [23] C.M.R.Fowler, The Solid Earth: An Introduction to Global Geophysics., Cambridge University Press, 2nd edition, 2005.
- [24] C. F. Gauß, Bestimmung des Breitenunterschiedes zwischen den Sternwarten von Göttingen und Altona durch Beobachtungen am Ramsdenschen Zenithsector, Vandenhoeck und Ruprecht, 1828.
- [25] F. G. Lemoine, S. C. Kenyon, J. K. Factor, R. Trimmer, N. K. Pavlis, D. S. Chinn, C. M. Cox, S. M. Klosko, S. B. Luthcke, M. H. Torrence, Y. M. Wang, R. G. Williamson, E. C. Pavlis, R. H. Rapp, T. R. Olson, The development of the joint nasa gsfc and nima geopotential model egm96.
URL <https://cddis.nasa.gov/926/egm96/egm96.html>
- [26] ESA, Goce.
URL https://www.esa.int/Enabling_Support/Operations/GOCE
- [27] ESA, A missão de gravidade da esa, goce, de novo operacional.
URL https://www.esa.int/Space_in_Member_States/Portugal/A_missao_de_gravidade_da_ESA_GOCE_de_novo_operacional
- [28] J.Johannessen, The Four Candidate Earth Explorer Core Missions-GRAVITY FIELD AND STEADY-STATE OCEAN CIRCULATION, ESA Publications Division, 1999.
- [29] C.W.Hughes, R.J.Bingham, An oceanographer's guide to goce and the geoid., Ocean Sciencedoi:
<https://doi.org/10.5194/os-4-15-2008>.
- [30] H.Wu, Gravity field recovery from GOCE observations, Fachrichtung Geodäsie und Geoinformatik der Leibniz Universität Hannover, 2016.
- [31] A.Jäggi, Precise Orbit Determination [PowerPoint Slides], Astronomical Institute-University of Bern, 2015.
URL https://boris.unibe.ch/72570/1/AJ_AutumnSchool15.pdf
- [32] J.Pilowsky, Estimating autocorrelation of colored noise.
URL <https://cran.r-project.org/web/packages/colorednoise/vignettes/noise.html>
- [33] H.Sünkel, GOCE: Preparation of the GOCE Level 1 to Level 2 Data Processing, Graz University of Technology, 2002.
URL <https://earth.esa.int/eogateway/documents/20142/37627/GOCE-Preparation-of-the-GOCE-Level-1-to-2-data-processing.pdf?>
- [34] O. Abrikosov, F. Flechtner, C. Förste., U. Meyer, M. Rothacher, R. Schmidt, Contribution of modern satellite tracking data to GOCE-based gravity solutions [POSTER], GeoForschungsZentrum Potsdam, 2006.
URL https://earth.esa.int/workshops/goce06/participants/131/poster_Poster_GOCE06.pdf
- [35] P. K. Kythe, Green's Functions and Linear Differential Equations: Theory, Applications, and Computation, Chapman and Hall/CRC, 2011.
- [36] C. R. Frye, C. Efthimiou, Spherical Harmonics in p Dimensions, World Scientific, 2012.
URL <https://arxiv.org/pdf/1205.3548.pdf>

Appendix A. Expansion in spherical harmonics and their completeness

As we have previously stated in section 3.2, any well behaved function dependent on the polar and azimuth angles can be expanded in a spherical harmonics series. But what is it meant when saying "well behaved"? Beyond the usual assumptions of a continuous function, with finite and single values across its domain, rises the clear necessity for the spherical harmonics series to converge in relation to the function we are representing using spherical harmonics in the first place! Therefore, in the sense of mean-square convergence, in order for the expansion expressed in equation 38 to be valid, it must fulfill the following limit [35]:

$$\lim_{n \rightarrow \infty} \int_0^{2\pi} \int_0^\pi |g(\theta, \phi) - \sum_{l=0}^n \sum_{m=-l}^l A_{lm} Y_{lm}(\theta, \phi)|^2 \sin \theta d\theta d\phi = 0. \quad (\text{A.1})$$

The functions capable of fulfilling this limit are called square-integrable functions. For the simplified one dimensional case, these functions, with domain D , and real (or complex) output value, are those for which the integral

$$\int_D f(x)^2 w(x) d\Omega \quad (\text{A.2})$$

exists and is finite (with respect to the weight, $w(x)$). In actuality, mean-square convergence is the same as convergence in L^2 , L^2 being the space of the aforementioned square-integrable functions. When endowed with the usual function operation properties and paired with the inner product

$$\langle f, g \rangle = \int_D f(x) g(x) w(x) d\Omega, \quad (\text{A.3})$$

the set of these functions forms an inner product space. It also turns out this space is complete, since it can be proven that every Cauchy sequence starting from this space converges to an element of said space. Finally, definition holds that a complete inner product space is called a Hilbert space. In sum, any square-integrable function can be expanded in spherical harmonics, and the space composed of all these functions is a Hilbert space [36].

The spherical harmonic functions then constitute a set in the inner product space of square-integrable functions. This being a Hilbert space inherits all its properties, a very important one being the following - an orthonormal set belonging to a Hilbert space is complete if and only if it is closed. We have stated before that the spherical harmonics set is orthogonal, and capable of being orthonormal with the introduction of a normalization factor. Thus, if we prove this set of functions is closed, we prove its completeness. A theorem can be given to assess if a set of functions (belonging to the Hilbert space) is closed. Let S denote the set of spherical harmonic functions and let f denote a generic continuous function of domain S^2 (the unit sphere) and real output. The theorem can be proved for f representing a square-integrable function, but the weaker version will be proved here. The theorem then

states that if f is orthogonal to the set S , i.e., if

$$\int_{\xi \in S^2} f(\xi) Y_{l,m}(\xi) d\Omega_2 = 0, \text{ for all } l, m \quad (\text{A.4})$$

then f is the zero function: $f(\xi) = 0$, for all $\xi \in S^2$ [36]. This theorem is proved by contradiction, i.e., assuming f satisfies the equation A.4 but it is not the zero function only to conclude the impossibility of that. This demonstration requires a deeper understanding of maths in order to fully grasp it, and since this a physics, not maths, essay, it doesn't seem necessary or urgent to understand all the mathematical steps that lead to the intended result. The demonstration is present in pages 78-79 of "Spherical Harmonics in p Dimensions", by "Christopher R. Frye and Costas Efthimiou," ([36]). The demonstration makes use of neighborhood continuity of functions, the Weierstrass approximation theorem and some concepts and definitions of the Legendre polynomials. With the proof that the set of spherical harmonic functions is indeed closed, it is finally proven that the set of spherical harmonic functions is complete.

Appendix B. Program Guide

Appendix B.1. Installation instructions

In this section, we will briefly indicate the steps required to install and run our computational application, as well as its capabilities.

1. Click on the link indicated on the email (<https://drive.tecnico.ulisboa.pt/download/1414448696233759>). This will open a google tab and will start to download a .zip file called "multipole_G4.zip".
2. Go to Downloads and copy the .zip file you just transferred for the folder where you want to run the program in.
3. Right click on the file and select the option to "Unzip here". This will take a few seconds and in the end will create a new folder named "multipole_G4".
4. Open the command window and on it, type "python -m pip install --upgrade pip" and press enter. This will take a few seconds. You can now close the command window.
5. Go to the folder you extracted in step 3. There you will find a file named "setup" or "setup.bat", depending on your file explorer settings. Press this file twice. This will install all the packages needed to run this program in a python environment. This will take about **5 minutes**. During this process, do not interact with nor close any command windows that pop up. In the end of this program, you may get an error regarding the directory name (it varies from computer to computer, but you can ignore this error). You should get a message that says "Hit any key to exit...". You should press any key and close the window.
6. Go back to the folder extracted in step 3 and refresh the file explorer. If all went according to plan, you now have a shortcut in this folder with the name "Multipole".
7. Press this shortcut twice to open the program. It will initially open a command window. Wait about 30 seconds. Do not interact with the command window during this time. The main program GUI will then appear as follows:

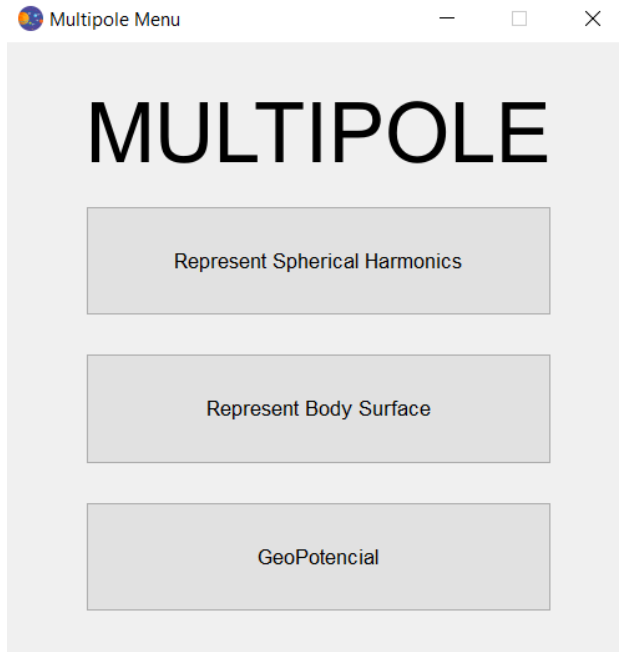


Figure B.38: Program GUI.

If at any step of this process you encounter any problem or if the final GUI window doesn't appear, please contact us so we can help you with the installation.

To close the program, you can either close the command window or the GUI.

Appendix B.2. Features

The program's main window comes with the following options:

- Represent Spherical Harmonics
- Represent Body Surface
- GeoPotential

In order to select each of these options, just click once on them and a new window will show up. In case you want to select other options, just close recently opened tab because the main window will be left opened.

Appendix B.2.1. Represent Spherical Harmonics

This section of the program allows the user to visualize the shape of the spherical harmonics functions. According to Fig.B.39:

1. Degree and Order: (Allows the user to select every spherical harmonics functions up to degree and order of 50).
2. Type: (Allows the user to select three different parts of the spherical harmonics functions: Absolute, Real and Imaginary).

3. Representation:(The user can visualize the true shape of the spherical harmonics (with the Ylm option), as well as its influence on the unit sphere. The different colors represent the distance to the origin. In addition to that, the sum of the last two representations can be visualized with the option (Ylm+1))
4. View along the axes (X+ X- Y+ Y- Z+ Z-) and Isometric view.
5. Toggle Parallel Projection, Toggle Axes Indicator and Toggle Full Screen.
6. Save Representation as a Screenshot and more options.

The user can use the mouse to rotate the figure about the origin. Further options include:

- CTRL+MOUSE: to rotate about a selected point.
- SHIFT+MOUSE: to move the figure.
- SCROLL WHEEL: to zoom in and out.

As the user explores the options, it might be seen that the program doesn't respond when the Imaginary option is selected along with $m=0$. This happens because the zonal harmonics don't have an imaginary part. That can be confirmed by the fact that the absolute value representation corresponds to the real one.

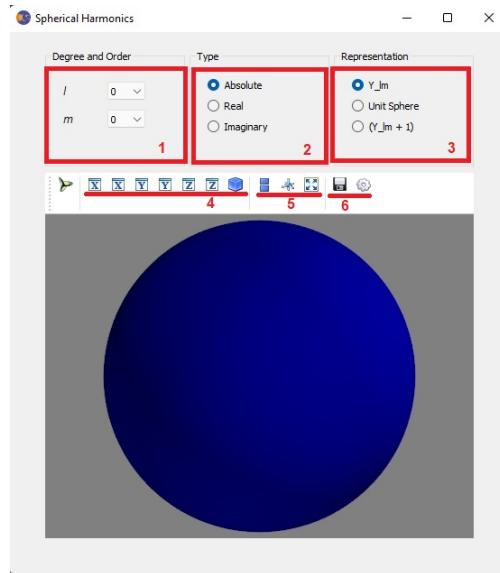


Figure B.39: Interface of "Spherical Harmonics Representation"

Appendix B.2.2. Represent Body Surface

This section of the program allows the user to visualize the spherical harmonics representation of a given irregular body and compare it to the original one. According to Fig.B.40, the present options are:

1. Body and Max Degree: the user is able to select one out of four irregular bodies which represent asteroids. They have all been retrieved from NASA's archives. The user can also select one of the available maximum degrees in which the body can be represented that we have calculated beforehand for ease of use.
2. Add New Max Degree: In this tab, the user has the freedom to select any maximum degree. By clicking "Calculate", the program will take some time to perform the calculations (explained in section 12) needed and then output the representation for the chosen degree. It should be noted that any new values of maximum degree that are calculated will be stored and these representations can be accessed in the "Max Degree" tab. **CAUTION:** the time taken to perform the calculations increases with the maximum degree for which we are approximating. Any input over 20 (depending on the machine) may cause the window to display "Non responding". If you wait long enough, it will eventually display the representation. Therefore, we do not recommend any input above 20.
3. Original Body: It shows the 3D representation of the original body extracted directly from the NASA archives.
4. Spherical Harmonic Representation: It shows the 3D representation of the body as a linear combination of all spherical harmonic coefficients up to degree and order L_{max} .

The user can use the MOUSE to rotate the body about the origin. It should be noted that both representations are affected by MOUSE operations. Further options include:

- CTRL+MOUSE: to rotate about the axis perpendicular to the screen.
- SHIFT+MOUSE: to move the figure.
- SCROLL WHEEL: to zoom in and out.

The program will not perform the calculations with invalid inputs such as letters or other special characters.

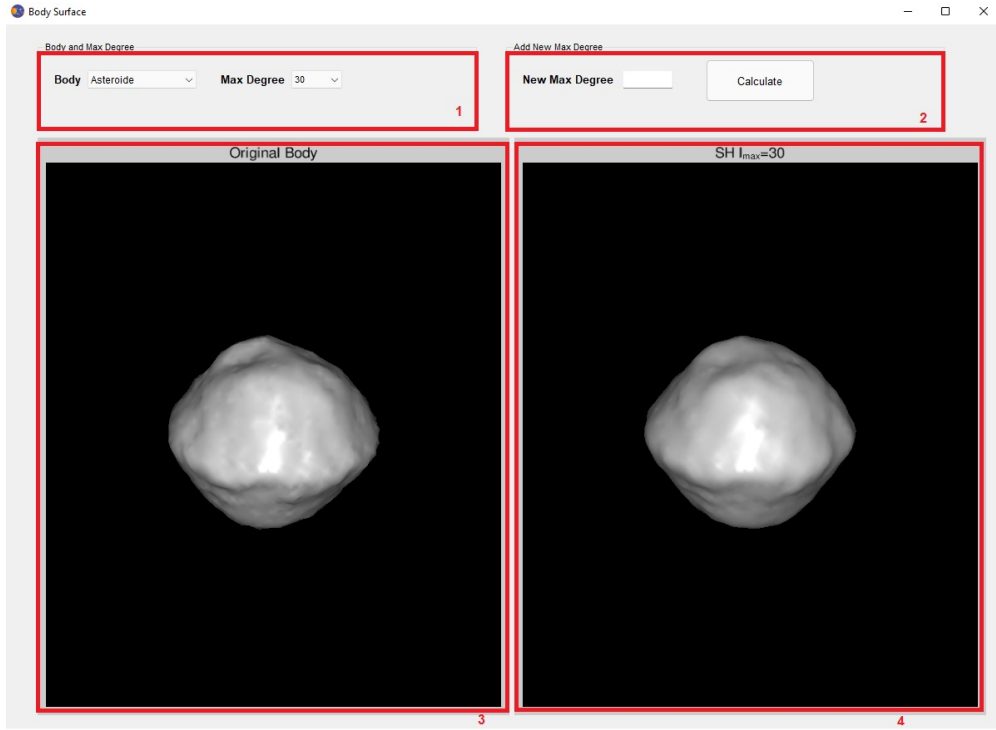


Figure B.40: Interface of "Body Surface"

Appendix B.2.3. GeoPotential

This section of the program allows the user to visualize different parameters along the Earth's surface and throughout the space around the Earth. It comes with five different tabs which allow the visualization and calculation of different parameters. Some of these parameters, such as the geoid heights, are described in more detail in section 10.4

- Geoid Here, we can visualize the geoid (also described in section 10.4), as calculated from coefficients obtained by a mission such as GOCE's.
 1. It comes with a colormap along the surface of the Earth which represent the geoid heights.
 2. The scale is represented in a colorbar.
 3. 3D representation of the Earth's geoid

The 3D body can be manipulated as follows:

- View along the axes (X+ X- Y+ Y- Z+ Z-) and Isometric view.
- Toggle Parallel Projection, Toggle Axes Indicator and Toggle Full Screen.
- Save Representation as a Screenshot and more options.

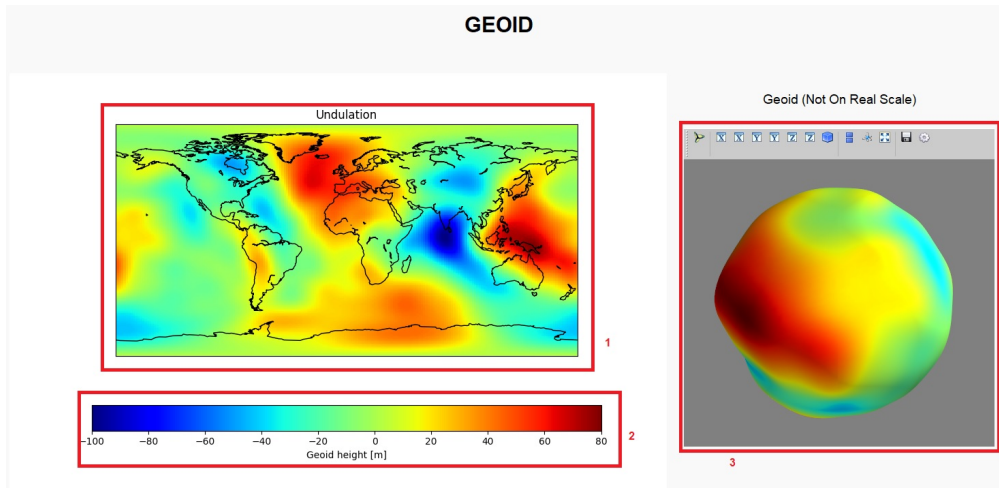


Figure B.41: Interface of "Geoid"

- Coefficients Visualization

In this part of the program, we display what the gravitational potential of the Earth would look like if the J2 coefficient was in a different position. In other words, we replace the actual value of the coefficient by the value that is usually in the J2 position. After sliding to the desired position and leaving it still, the image will change shortly.

1. Colormap of the Gravitational Potential in a Sphere of Radius of 6378km along its colorbar with the respective scale.
2. Colormap of the Gravitational Acceleration in a Sphere of Radius of 6378km along its colorbar with the respective scale.
3. Replace J2 coefficient: the slider allows the user to replace the J2 coefficient by one of the ten available (C52 would refer to the coefficient of degree 5 and order 2).

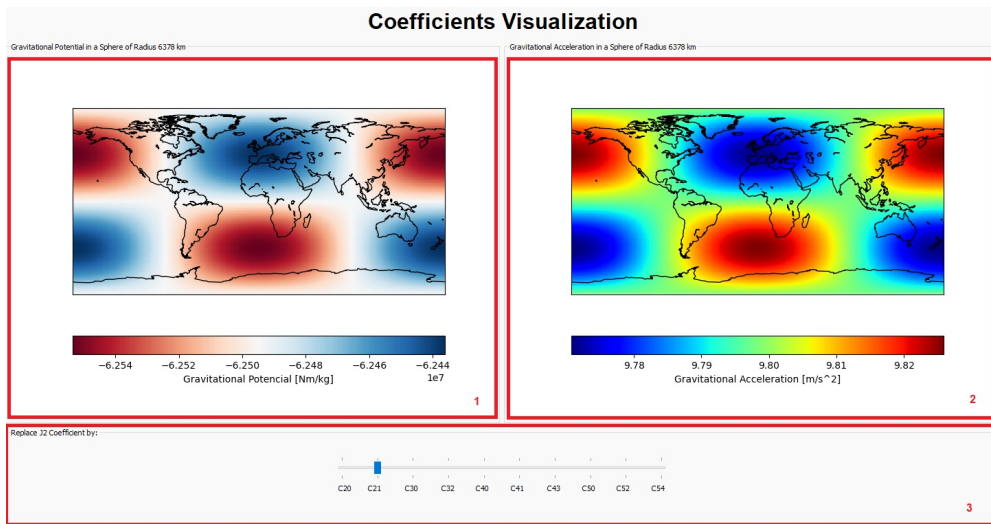


Figure B.42: Interface of "Coefficients Visualization"

- Potential Visualization

In this section, we perform an analysis of the potential field around the planet, both as a sphere around the Earth and in an equatorial cut.

1. Colormap of the Gravitational Potential on a Sphere of Radius of 6378km along with a colorbar which indicates the corresponding scale. This section also comes with a slider which allows the user to select different heights from 220km to 230km.
2. Colormap of the Gravitational Potential on a slice of Sphere of Radius of 6378km along its colorbar with the corresponding scale. This slice corresponds to the intersection of the sphere with a plane with polar angle of 0 degrees. Adjusting the slider allows the user to visualize the potential distribution from the Earth's radius to the selected height.

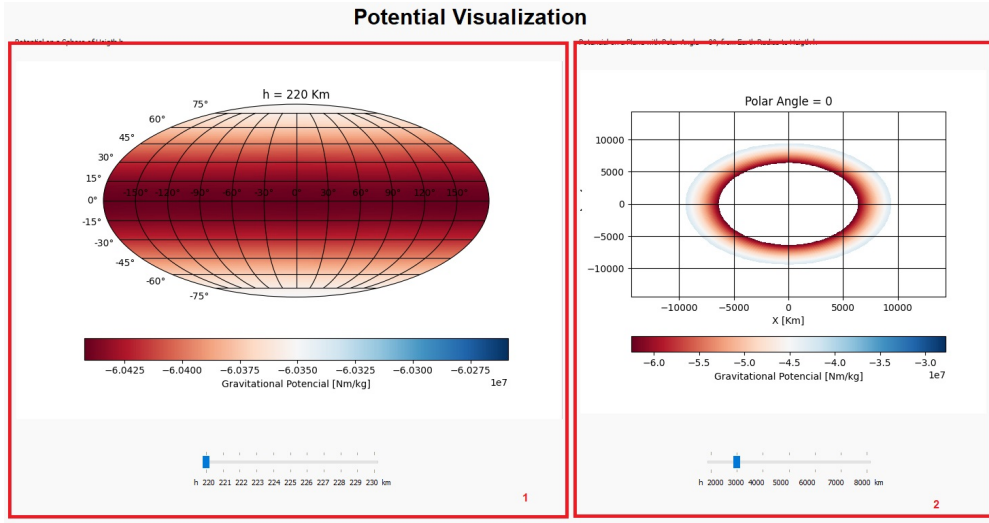


Figure B.43: Interface of "Potential Visualization"

- Acceleration Visualization

Similarly to the last section, here we plot the acceleration values around the planet.

1. Colormap of the Gravitational Acceleration on a Sphere of Radius of 6378km along with a colorbar which indicates the corresponding scale. This section also comes with a slider which allows the user to select different heights from 220km to 230km
2. Colormap of the Gravitational Acceleration on a slice of Sphere of Radius of 6378km along its colorbar with the corresponding scale. This slice corresponds to the intersection of the sphere with a plane with polar angle of 0.057 degrees due to a singularity at 0 degrees. Adjusting the slider allows the user to visualize the acceleration distribution from the Earth's radius to the selected height.

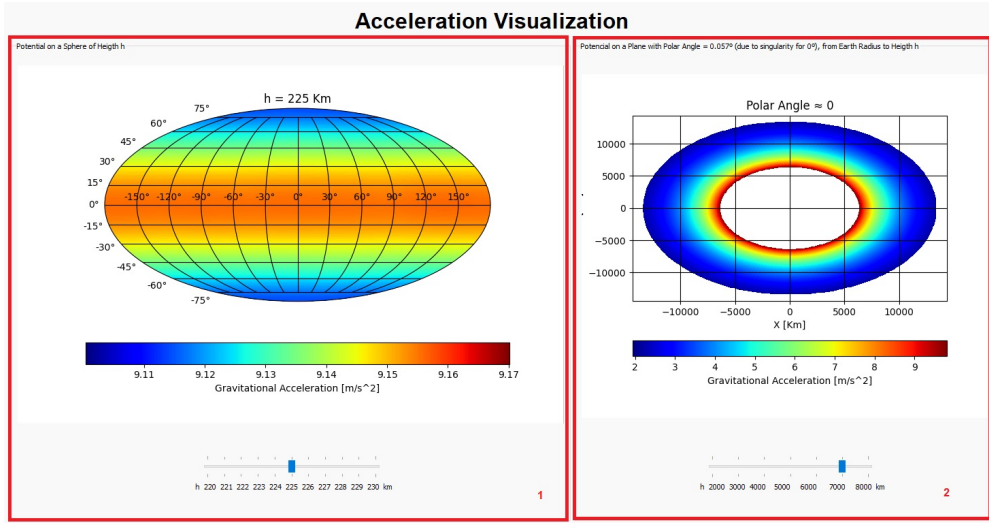


Figure B.44: Interface of "Acceleration visualization"

- Calculate Gravitational Potential & Acceleration

Here, we calculate the gravitational potential and acceleration for an individual point that is specified by polar and azimuth angles, as well as by the height above the perfect sphere of radius 6378.

1. Colormap of the Gravitational Potential (left) and Gravitational Acceleration (right) on a perfect sphere of radius of $6378 + h$ km (h being the altitude input by the user) along with colorbars which indicate the corresponding scales. Notice that changing the altitude the figures themselves don't change, only the scales do (this is because we set the colorbar's limits to automatic).
2. Coordinates of the point where the potential and acceleration are to be computed. These are represented in spherical coordinates: Height, Polar Angle and Azimuth Angle. Each parameter comes with an interval in which the calculations yield valid results. The program will not run with invalid inputs and the input will return to the last valid input (if an invalid input is entered).
3. Results of the calculations performed by the program as a function of the selected inputs. The black dot in each graph indicates the selected coordinates.

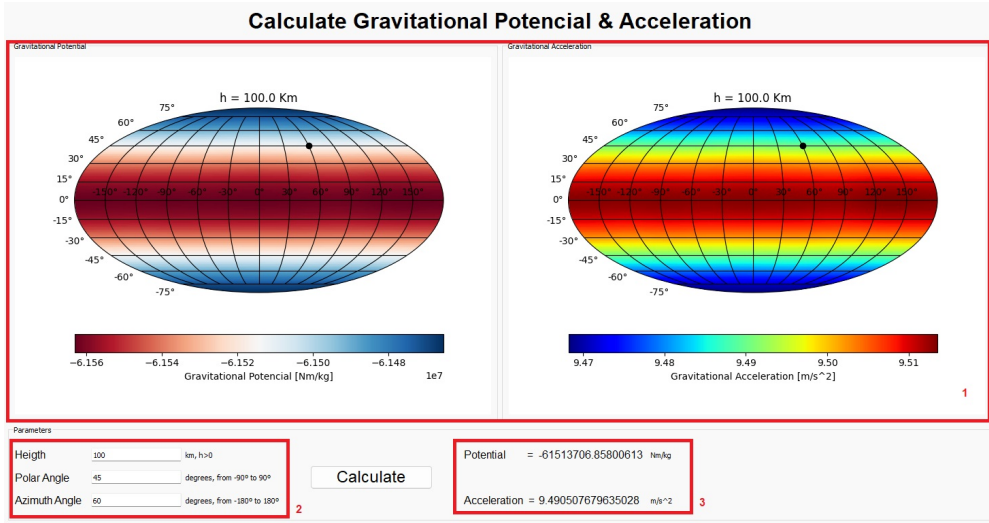


Figure B.45: Interface of "Calculate Gravitational Potential & Acceleration"

Appendix C. Group qualitative assessment

Finally, we present a qualitative evaluation by the group of each member's individual contributions. The scale used is 0, ± 1 , ± 2 , where zero is an average contribution and ± 2 are far from average. We also present the sections that each member tended to:

- Alano Silva → 0: Sections 2, 2.1, 4 and 5;
- Diogo Faustino → 0: Sections 1 and 6;
- Henry Machado → +1: Section 15, Appendix B.2 and Computational Program;
- João Soeiro → 0: Sections 7, 9, 16, and plots for gravitational field for different density models (Section 8, figure 14);
- José Bento → +1: Sections 10.2, 10.3, 10.4, 13, 14, Appendix B.1 and Computational Program;
- Rúben Novais → 0: Sections 2.1, 3 and Appendix A;
- Tomás Nunes → +1: Sections 11, 12, Appendix B.1 and Computational Program;
- Rodrigo Sequeira → 0: Sections 8, 10, 10.1, 16 and plots for gravitational field for different density models (Section 8, figure 14).